Nature of Ferroelectric Behavior in Main-Chain Dipolar Glass Nylons: Cooperative Segmental Motion Induced by High Poling Electric Field

Zhongbo Zhang, Morton H. Litt, and Lei Zhu*

Department of Macromolecular Science and Engineering and Department of Chemistry, Case

Western Reserve University, Cleveland, Ohio 44106-7202, United States

Corresponding authors. Email: lxz121@case.edu (L. Zhu), Tel. +1 216-368-5861

Abstract

Main-chain dipolar glass polymers such as aromatic nylons are promising for high energy

density and low loss dielectric applications because of the limited, non-cooperative oscillation of

highly dipolar amide groups. However, quenched aromatic nylons have been reported to exhibit

significant ferroelectric switching upon high field poling. It is desirable to suppress ferroelectric

switching for electric energy storage application, and this requires a fundamental understanding of

the nature of ferroelectric behavior in dipolar glass nylons. In this work, a nearly 100% amorphous

aromatic nylon, Selar, was used to investigate the origin of ferroelectricity in glassy nylons. Using

Fourier transform infrared spectroscopy, it was found that hydrogen-bonding strength played an

important role in the ferroelectric switching of amide dipoles in the loosely packed glassy matrix.

When hydrogen-bonding was weak such as in the quenched film, significant ferroelectric

switching took place. In contrast, quenched and annealed films did not exhibit any ferroelectric

switching. High-voltage broadband dielectric spectroscopy was used to study molecular and

segmental motions in Selar. It was observed that the primary contribution to ferroelectric

switching came from cooperative segmental motions (i.e., a combination of various sub-T_g

relaxations, where Tg is the glass transition temperature) in the main-chain dipolar glass nylon.

This understanding will help us design new aromatic nylons with suppressed segmental motions

for high energy density and low loss dielectric applications.

Keywords: sub-Tg transitions, glassy aromatic nylons, ferroelectric switching, Selar

2

Introduction

High dielectric constant (ε_r) and low loss dielectric polymers are attractive for advanced electrical and power applications, such as electric energy storage (i.e., film capacitors), ¹⁻³ electromechanical actuation (i.e., dielectric elastomers^{4, 5} and electrostrictive polymers⁶), and electrocaloric cooling. ⁷⁻⁹ From recent studies, ^{1, 10} enhanced dielectric constant for polymers can be realized by utilizing orientational (or dipolar) polarization from dipolar groups, such as nitrile (3.9 D), sulfone (4.5 D), amide (3.7 D), urea (4.5 D), and thiourea (4.89 D) groups. According to different dipole-dipole and domain-domain interactions, dipolar polymers can be categorized into four types; normal ferroelectric, relaxor ferroelectric, paraelectric, and dipolar glass polymers. ^{1, 3} Among these, a promising candidate is the dipolar glass polymer, where weakly interacting dipolar groups are confined in the glassy polymer matrix. ^{1, 11} It is the free volume that permits dipole mobility below the glass transition temperature (T_g, i.e., sub-T_g transitions). ¹² Since the long-range segmental motion of polymer chains is largely frozen below T_g, ionic and electronic conduction losses can be significantly reduced. ^{11, 13}

Two sub-categories have been observed for dipolar glass polymers. The first involves polymers with nearly 180° -rotation of side-chain dipolar groups such as cyanoethyl (or cyanomethyl)¹³⁻¹⁷ and methylsulfonyl groups. High dielectric constants in the range of 4-15 have been reported for these polymers below T_g . Current research efforts are dedicated to achieving low dielectric loss (e.g., dissipation factor, $\tan \delta < 0.01$) within a broad temperature window. Namely, the sub- T_g transition should take place at a low enough temperature (< -50 °C), and the T_g should be high (>200 °C). The second sub-category involves main-chain polymers with limited, non-cooperative oscillation of strongly dipolar groups in the main chain. Sometimes, it is difficult to differentiate the dipolar oscillation from the infrared vibration, which actually

belongs to the atomic or vibrational polarization.²⁰ An example is the all-aromatic polythiourea with a large dipole moment per repeat unit.²¹⁻²⁵ The dielectric constants for these polythioureas are lower than those for the first sub-category polymers, only about 4-6, due to the small-amplitude oscillation of dipolar groups. However, the dielectric loss can be rather low for these polythioureas. Under a high poling electric field of 1 GV/m, the energy density can reach as high as ~22 J/cm³.²¹

In this work, we explore the opportunity of aromatic polyamides (PAs or nylons) as an alternative to aromatic polythioureas, because many aromatic nylons are commercially available, e.g., MXD and Selar. Nylon MXDs are synthesized from *m*-xylylenediamine and aliphatic dicarboxylic acids with methylene numbers varying from 6 to 13. Most MXDs are amorphous upon quenching from the melt, but become semicrystalline after annealing at high temperatures. Selar, usually an amorphous copolymer, is prepared from hexamethylenediamine (HMD) and a combination of isophthalic acid (I) and terephthalic acid (T). In literature reports, Selar was also named as copolymer 6I/T (where 6 means HMD). When the I/T composition is 70/30 mol./mol., Selar is nearly 100% amorphous with a Tg around 129 °C. However, amorphous MXDs and Selar nylons (and also alicyclic nylons) have been reported to show ferroelectric switching behavior with broad hysteresis loops. Although the ferroelectric switching is attributed to the amorphous dipoles in the glassy polymer matrix, Its detailed mechanism has not been clearly understood.

Recent studies demonstrate that the ferroelectric switching in aliphatic *n*-nylons originates primarily from the mesomorphic crystalline structure in the melt-quenched polymer,³² rather than from the pure amorphous phase as reported before,³³⁻³⁶ regardless of odd- or even-numbered *n*-nylons. This observation for aliphatic *n*-nylons seems to contradict the report of ferroelectric behavior in glassy aromatic (and alicyclic) nylons. Because ferroelectric switching is not desired

for electric energy storage applications, it is important for us to understand the underlying mechanism of ferroelectric switching in glassy aromatic nylons and to suppress it as much as possible. Otherwise, it would be very difficult to develop viable aromatic polyamide alternatives for the high energy density and low loss aromatic polythioureas.

Experimental Section

Materials. Selar resin was purchased from DuPont (Wilmington, DE). Nylon-12 and nylon-6 resins were purchased from Sigma-Aldrich (St. Louis, MO, U.S.A.). Nylon-11 resin (Arkema Rilsan® Besno TL) was purchased from PolyOne (Avon Lake, OH, U.S.A.). All nylons were used as received without further purification, except for thorough drying in a vacuum oven at 70 °C for 3 days before hot-pressing and dielectric property characterization.

Film Fabrication and Processing. Five types of film samples were fabricated for this study. (1) Quenched (Q) samples. Sandwiched with aluminum foils, Selar was heated at 250 °C and *n*-nylon samples were melted at a temperature about 30-40 °C above their melting temperatures (T_m, i.e., 210 °C for nylon-11 and nylon-12, and 250 °C for nylon-6). During hotpressing, a compression force of 10 tons was applied, and sample thickness was controlled to be approximately 20-25 μm. After hot-pressing, the aluminum foil-sandwiched samples were immediately quenched into an isopropanol/dry ice bath (about -78 °C). (2) Quenched and annealed (QA) samples. For *n*-nylons, the Q samples were annealed at 140 °C for 12 h in a vacuum oven to obtain the most stable crystalline forms. The Q Selar sample was annealed at 110 °C for different lengths of time: 1 h (QA-1h), 3 h (QA-3h), 6 h (QA-6h), 12 h (QA-12h), 24 h (QA-24h), and 72h (QA-72h). (3) Quenched and stretched (QS) samples. The Q nylon samples were uniaxially stretched at RT to an extension ratio of ca. 300%, using a home-built stretching

apparatus. (4) Quenched, stretched, and annealed (QSA) samples. The QS Selar samples were annealed in a vacuum oven at $110\,^{\circ}$ C for $12\,h$. (5) Solution-cast and annealed (CA) samples. Selar was dissolved in redistilled trifluoroethanol (TFE). The film was cast onto a glass slide substrate, which was pre-coated with gold as the bottom electrode. The thickness of the CA film varied from 3 to 8 μ m, depending on the concentration of the solution (25-50 mg/mL). The CA film was dried in air for about 4 h, followed by annealing at $110\,^{\circ}$ C in a vacuum oven for additional 72 h.

Instrumentation and Characterization. Fourier transform infrared (FTIR) spectra were recorded using a Nicolet iS50R FTIR spectrometer (Thermo Fisher Scientific, Waltham, MA) in the transmission mode. The scan resolution was 2 cm⁻¹ with 64 scans. Differential scanning calorimetry (DSC) was performed using a TA Instruments Q2000 DSC at a scanning rate of 10 °C/min. Around 1.5 mg of samples were used in DSC to avoid any thermal lag.

Two-dimensional (2D) wide-angle X-ray diffraction (WAXD) measurements were carried out using a Rigaku MacroMax 002^+ equipped with a Confocal Max-Flux® optic and a microfocus X-ray tube source operating at 45 kV and 0.88 mA. The X-ray wavelength was 0.1542 nm (Cu K α). The WAXD patterns were collected using a Fujifilm image plate scanned by a Fujifilm FLA-7000 scanner at a resolution of 50 μ m/pixel. The sample-to-detector distance was calibrated using silver behenate, whose first order reflection is located at the scattering vector (q) of 1.076 nm⁻¹ [q = $(4\pi \sin\theta)/\lambda$ with θ being the half scattering angle]. One-dimensional (1D) WAXD curves were obtained by integrating the corresponding 2D WAXD patterns using the Polar software developed by Stonybrook Technology and Applied Research, Inc.

Electric displacement-electric field (D-E) loop measurements were performed using a Premiere II ferroelectric tester (Radiant Technologies, Inc., Albuquerque, NM) in combination with a Trek 10/10B-HS high-voltage amplifier (0-10 kV AC, Lockport, NY). The applied voltage

had a bipolar sinusoidal or triangular waveform in the frequency range of 10-1000 Hz. Gold (Au) electrodes (2.4 mm diameter and ca. 10 nm thick) were evaporated onto both sides of the film sample using an EvoVac Deposition System (Angstrom Engineering, Inc., Kitchener, ON, Canada). The metallized films were immersed in silicone oil (Fisher 460-M3001) during D-E loop testing to avoid corona discharge. The temperature was controlled by an IKA RCT temperature controller (Wilmington, NC). A home-built sample fixture with high-voltage cables was used to connect the electrodes on the films to the interface of Radiant ferroelectric tester.

Temperature-scan broadband dielectric spectroscopy (BDS) measurements were performed using a Novocontrol Concept 80 dielectric spectrometer with the frequency ranging from 0.01 to 10^6 Hz and the temperature ranging from -150 to 140 °C at 1.0 V_{rms} (i.e., root-mean-square voltage). High voltage BDS (HV-BDS) measurements were performed on a Novocontrol Concept 80 broadband dielectric spectrometer with a high-voltage interface, HVB4000. The interface could provide up to ± 2000 (peak-to-peak) V_{AC} with the frequency up to 10^4 Hz. Samples were heated at 0.3 °C/min. Meanwhile, the frequency was scanned between 10 and 10^4 Hz and the electric field scanned from 3.2 to 33.2 MV/m.

Results and Discussion

Comments on Ferroelectric Behavior in Aliphatic Nylons. Before discussing the nature of ferroelectric switching in glassy aromatic nylons, it is necessary to review the ferroelectric behavior in aliphatic nylons. First, using a common cooling/quenching process (i.e., a cooling rate <300 °C/min), it is not possible to quench *n*-nylons into a complete amorphous phase.^{37,38} Instead, they exhibit a mesomorphic crystalline phase with relatively low crystallinity (ca. 20-25 wt.%).^{32,38} In this mesophase, the aligned chains have a highly twisted chain conformation. Amide

groups from neighboring chains organize into a smectic-like structure with disordered hydrogen bonds, and thus the hydrogen-bonding interaction is weak. The mesophase is so poor that WAXD only shows an amorphous halo-like broad scattering at high scattering vector q of ~14.7 nm⁻¹ and a smectic reflection at low q of 4-8 nm⁻¹. Especially for mesomorphic (i.e., quenched) nylon-6, the low q reflection was rather weak.³² Such a WAXD profile was easily mistaken as the one from 100% amorphous nylons;³³⁻³⁶ however, this is incorrect, because if the quenched n-nylons are completely amorphous, the smectic reflection around 4-8 nm⁻¹ should not show.

Second, the mesophase in quenched *n*-nylons enables the dynamic, field-induced ferroelectric behavior because of weakened hydrogen-bonding, whether in odd- or even-numbered *n*-nylons. Therefore, polar crystalline structure is not a prerequisite for ferroelectricity in aliphatic nylons. However, there is an obvious difference between odd- and even-numbered nylons. Mesomorphic crystals in odd-numbered nylons favor the formation of ferroelectric domains, which continue to grow larger upon extended electric poling, resulting in broad D-E hysteresis loops. These field-induced ferroelectric domains are very stable and the Curie transition is above the T_m. Mesomorphic crystals in even-numbered nylons disfavor the formation of ferroelectric domains, because polymer chains need to be twisted more by the poling field in order to align neighboring amide bonds in the same direction to form ferroelectric domains. As a result, only transient (or short-lived) domains form and relatively narrow D-E hysteresis loops are obtained at room temperature (RT).

Third, further studies demonstrate that the mesomorphic structure is not the main enabler for ferroelectric switching of amide dipoles in aliphatic nylons. Instead, it should be the weakened hydrogen-bonding interactions in the mesophase. For example, only 5 min annealing at 100 °C of the mesomorphic/quenched *n*-nylon samples led to significant suppression of the ferroelectric

switching. WAXD and FTIR; however, hydrogen-bonding strength in the mesophase must have enhanced to suppress the ferroelectric switching. Strong hydrogen-bonding interactions also account for the non-ferroelectric behavior of well-annealed nylon crystals, including the α -form in odd-numbered nylons and the γ -form in even-numbered nylons (note that the α - and γ -forms can coexist in nylon-6 with the α -form being slightly more stable). From the above studies, the amorphous phase in aliphatic nylons was considered as paraelectric, and the ferroelectric switching originated primarily from the mesomorphic crystalline phase.

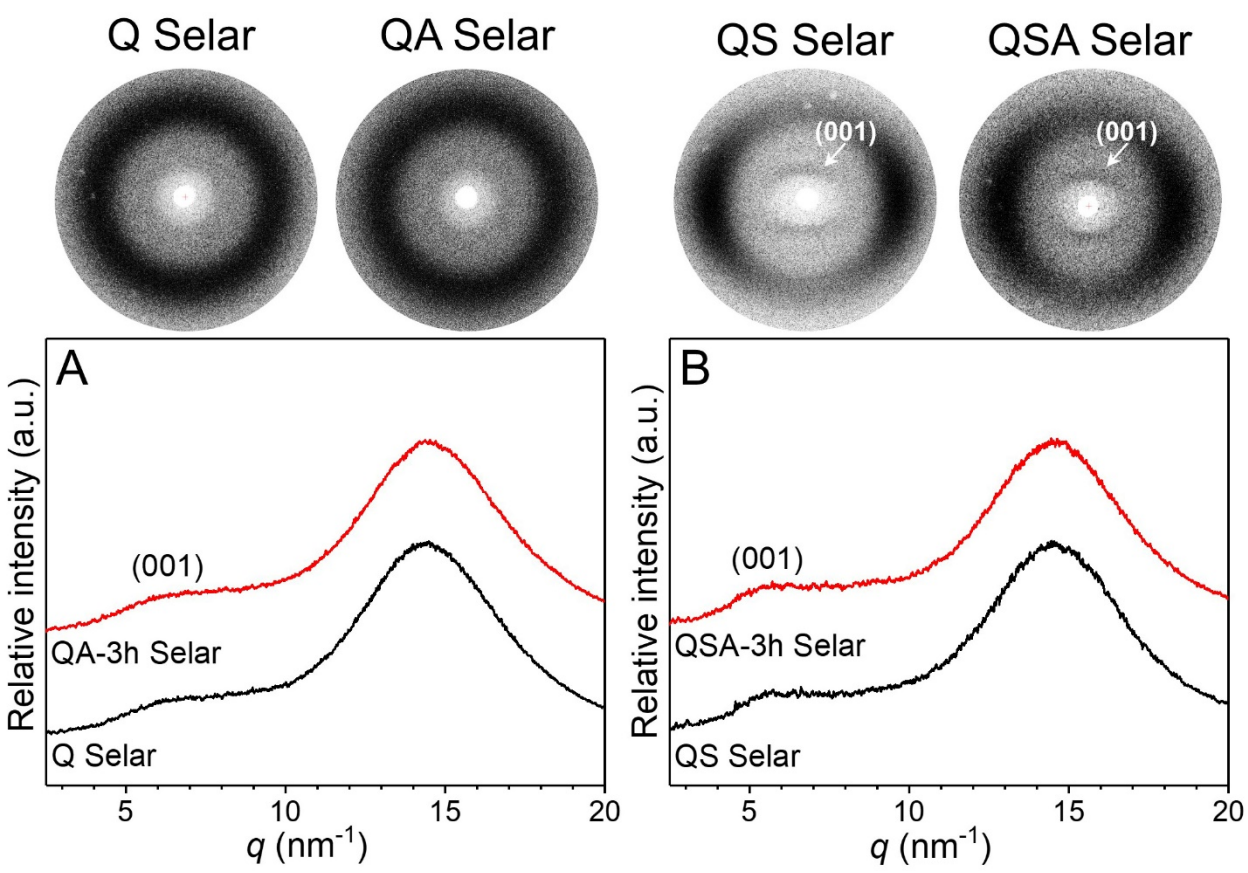


Figure 1. Room temperature 2D WAXD patterns and 1D WAXD profiles for (A) Q and QA-3h and (B) QS and QSA Selar films at room temperature.

Ferroelectric Behavior in Nearly 100% Amorphous Aromatic Nylons. In this study, Selar was chosen to study ferroelectric switching in glassy aromatic nylons, because unlike MXDs, Selar could remain largely amorphous even after high temperature annealing. Four samples were prepared; i) Q, ii) QA, iii) QS, and iv) QSA Selar films. The 2D WAXD patterns and the corresponding 1D WAXD profiles are shown in Figure 1. Although Selar was often reported as 100% amorphous in the past, 27, 29 our WAXD result showed that both Q and QA Selar films were not 100% amorphous. In addition to the amorphous halo at 14.5 nm⁻¹, a weak reflection was found at a low q around 6.0 nm⁻¹. This WAXD profile is fairly similar to that for quenched nylon-6.32After stretching, the QS (and the QSA) Selar film exhibited a horizontal streak-like reflection at a low q of 5.5 nm⁻¹ and an oriented amorphous halo around 14.5 nm⁻¹ (see the top right panel of Figure 1). From these WAXD results, the low q reflection could be attributed to the smectic-like organization of amide groups in the crystalline phase. The horizontal streak-like reflection in 2D WAXD patterns indicated that there was certain fluctuation of the smectic-like stacking along the drawing direction. Similar horizontal streak-like reflection was also observed for oriented poly(vinyl alcohol)/iodine complex crystals, where the I₃⁻ ions had a poor registry in the direction perpendicular to the drawing direction.⁴² Because of this horizontal streak-like reflection, the 1D WAXD profile did not show a well-defined peak for the smectic-like stacking. Instead, a stepwise peak was observed in Figure 1. Given the broad reflection at 14.5 nm⁻¹, the Selar crystals were probably in the mesomorphic phase, and then the low q peak was assigned as the (001) reflection (i.e., the chain direction). In addition, DSC of Selar showed a fairly weak melting peak around 250 °C for Selar. 43 From both WAXD and literature DSC results, we estimate that Selar should have a rather low crystallinity of only a few percent (note that an accurate determination of crystallinity was impossible because the heat of fusion for the perfect crystal is unknown). If the

I/T composition was changed to 35/65 mol./mol., the nylon copolymer became semicrystalline with a T_m around 330 °C.⁴³ Therefore, the crystallinity in the 6I/T copolymers should originate from 6T sequences. For the following ferroelectric study, Q and QA Selar samples were used, because QS and QSA films were found to significantly shrink after several times of ferroelectric switching cycles by high poling fields (note that even when both ends were fixed during thermal annealing, film shrinkage still happened after bipolar poling). We consider that stretching enhanced chain orientation for easier dipole switching, which increased heat generation when amorphous dipoles and domains were switched back and forth by the high poling field.

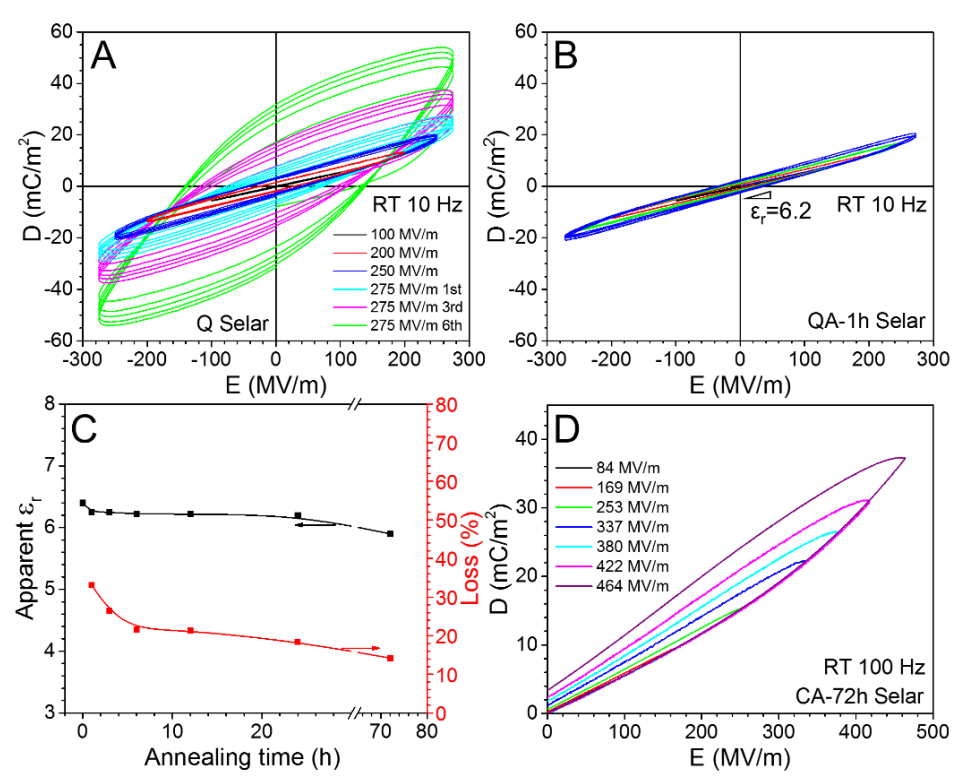


Figure 2. (A-B) Continuous bipolar D-E loops (5 loops for each run) at room temperature for (A) Q and (B) QA-1h Selar films under different electric fields; 100, 200, 250, and 275 MV/m. The poling frequency was 10 Hz with a sinusoidal waveform. For the Q film at 275 MV/m, six sets of five (6×5) continuous loops were applied. The time interval between two consecutive runs was ca. 30 s. (C) Apparent ε_r at 100 MV/m and hysteresis loop loss% at 275 MV/m as a function of annealing time for various QA Selar films. (D) Unipolar D-E loops at room temperature for the CA-72h Selar film under different poling fields. The poling frequency was 100 Hz with a triangular waveform.

The ferroelectric behavior for the Q Selar film was first studied using bipolar D-E loop tests at RT. For each bipolar poling, five continuous loops were performed to show the progress toward the steady state. The time interval between consecutive runs was ca. 30 s (i.e., the time for the Radiant tester to setup the next run). Figure 2A shows D-E loops for the Q Selar film under different poling fields at RT. When the poling field was below 250 MV/m, only linear loops were observed, although the loops gradually opened up as the maximum poling field increased. When the maximum poling field increased to 275 MV/m, ferroelectric switching started to develop and eventually became significant after 30 (i.e., 6×5) loops (see Figure 2A). Note that steady state and dipole saturation were not reached even after 30 loops at 275 MV/m and 10 Hz.

After annealing the Q film at 110 °C for just 1 h, the QA-1h Selar film exhibited linear D-E loops up to 275 MV/m (Figure 2B), indicating dramatic suppression of the ferroelectric switching. With further annealing at 110 °C up to 72 h, the D-E loops became increasingly slimmer (see Figure S1 in the Supporting Information). The apparent ε_r was obtained from the steady-state linear loop at 100 MV/m, and it slightly decreased from 6.4 to 5.9 after annealing at 110 °C for 72 h. Meanwhile, the hysteresis loop loss% at 275 MV/m dropped from 33% to 14% (Figure 2C; the calculation of hysteresis loop loss is given in ref. 11). The suppression of ferroelectric switching upon high temperature-annealing was also reported previously; however, the exact reason was still unclear.^{31, 43} One possibility could be a decrease in free volume upon physical aging at a temperature slightly below T_g .⁴⁴ As shown in the first heating DSC curves in Figure S2A, the QA Selar films did not show a significant hysteresis peak until the annealing time was beyond 6 h. This result indicated that the decrease in free volume could account for the decreases in ε_r and loss% after annealing at 110 °C for a prolonged time (e.g., 72 h; see Figure 2C),

but might not be the major reason for suppressed ferroelectric switching only after 1 h annealing (Figure 2B). Note that the suppressed ferroelectric switching after 1 h annealing at 110 °C for the Q Selar film is similar to that for the mesomorphic *n*-nylons after 5 min-annealing at 100 °C.⁴⁰ It is possible that enhanced hydrogen-bonding upon thermal annealing suppressed the ferroelectric switching for the QA Selar films, and this will be discussed later.

The QA Selar films were further subjected to even higher field poling (>275 MV/m) to see if ferroelectric switching could return or not. However, all QA films broke down rapidly when the poling field was above 300 MV/m at 10 Hz. Because of this, a thinner CA-72h film (3-8 μm) was used, and the poling frequency was increased to 100 Hz. However, no significant ferroelectric switching was observed for the bipolar poling up to 340 MV/m (Figure S2B), above which the CA-72h film broke down. Therefore, unipolar poling was applied, because it was reported that DC breakdown strengths were higher than the AC breakdown strengths especially for polar polymer films.⁴⁵ Figure 2D shows the unipolar D-E loops for the CA-72h film at RT and 100 Hz. Significant ferroelectric switching was observed when the poling field reached 464 MV/m. Note that RT is far below the T_g of Selar, and electronic and ionic conductions could be neglected. This result is different from the case for the aromatic polythiourea,²¹ which did not exhibit ferroelectric switching even when the poling field reached as high as 800 MV/m at RT and 10 Hz. It was possible that the hydrogen-bonding in polythiourea was stronger than that in the CA-72h Selar film, and thus prevented ferroelectric switching under high fields.

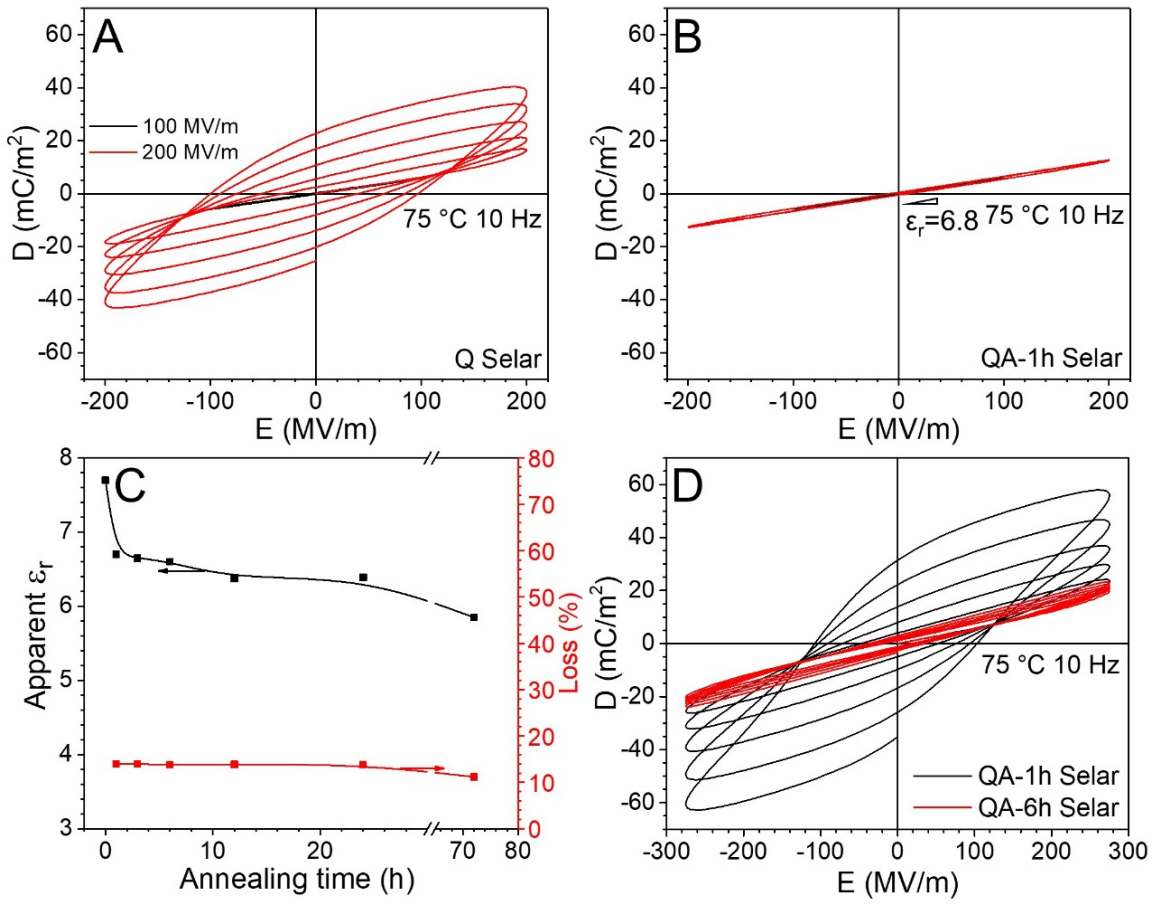


Figure 3. (A-B) Continuous bipolar D-E loops (5 loops for each run) at 75 °C for (A) Q and (B) QA-1h Selar films under different electric fields; 100 and 200 MV/m. The poling frequency was 10 Hz with a sinusoidal waveform. (C) Apparent ε_r at 100 MV/m and hysteresis loop loss% at 200 MV/m as a function of annealing time for various QA Selar films. (D) Continuous bipolar D-E loops at 75 °C for QA-1h and QA-6h Selar films under 275 MV/m. The poling frequency was 10 Hz with a sinusoidal waveform.

When the test temperature increased to 75 °C, ferroelectric switching became easier. For example, ferroelectric switching started during the first 5 loops for the Q Selar film when the poling field was only 200 MV/m (Figure 3A). The easier ferroelectric switching could be attributed to the weaker hydrogen-bonding interaction at elevated temperatures, as reported in a previous FTIR study on Selar. Because of the weakened hydrogen-bonding interaction, the lifetime of field-induced ferroelectric domains was expected to be relatively short. Figure 4 shows the lifetime results for the field-induced ferroelectric domains in Q Selar polarized at RT and 75 °C,

respectively. Before the lifetime test, the fresh Q Selar film was bipolarly polarized for five continuous cycles (275 MV/m at RT and 200 MV/m at 75 °C) to induce ferroelectric domains. During the lifetime test, the sample was polarized for one cycle, and then the electric field was held at 0 MV/m for additional 22 s (Figure 4A; the holding time is limited by the ferroelectric tester to be within 25 s). Figure 4B shows the -P_r as a function of time after one cycle of poling, i.e., 275 MV/m at RT and 200 MV/m at 75 °C. From the linear plot in the inset, there was a quick decrease in -P_r within the first 2 s, after which the decrease became gradual. The quick decrease of -P_r within 2 s could be primarily attributed to randomization of poled ferroelectric domains, and the gradual decrease could be a result of the disappearance of field-induced ferroelectric domains. If plotted in double logarithmic scales, the gradual decrease of -P_r seemed to follow a linear trend. It was obvious that the gradual decrease at 75 °C was faster than that at RT, and this could be attributed to faster thermal motion at higher temperatures. If linear extrapolation was valid (see the dashed lines in Figure 4B), the decay times (τ_d) for the -P_r (defined as the |P_r| decreasing to 1/e of the original value) would be ca. 5000 and 50 s at RT and 75 °C, respectively. Later, we will discuss possible molecular/segmental motions, which lead to the disappearance of field-induced ferroelectric domains in poled Q Selar films.

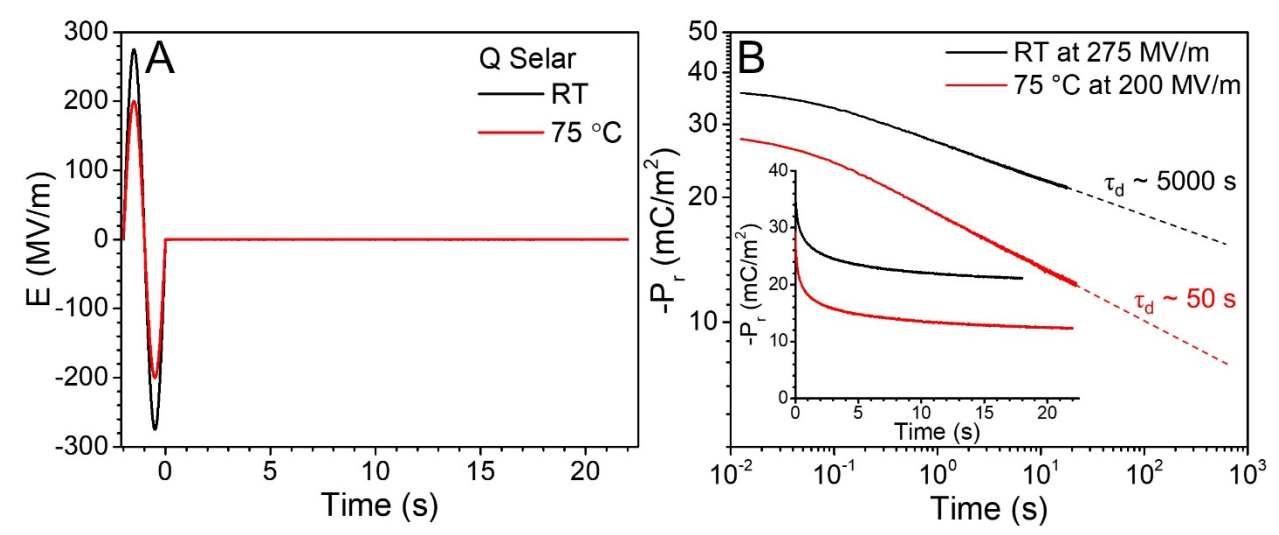


Figure 4. (A) Poling electric field profiles for the lifetime tests at RT and 75 °C for the Q Selar film. For the lifetime test, time started to count after one cycle of poling. (B) Double logarithmic plot of -P_r as a function of time for the Q Selar film at RT and 75 °C, respectively. The inset shows the linear plot.

After thermal annealing, e.g., for the QA-1h Selar film, ferroelectric switching at 75 °C was significantly suppressed under 200 MV/m (Figure 3B). Upon increasing the annealing time, D-E loops became increasingly slimmer (see Figure S3). The apparent ϵ_r at 100 MV/m and the loop loss% at 200 MV/m decreased with increasing the annealing time (Figure 3C). However, ferroelectric switching could be achieved at a higher poling field. For example, when the poling field increased to 275 MV/m, the QA-1h film still exhibited broad ferroelectric switching at 75 °C after 5 continuous poling loops (Figure 3D). When the annealing time increased to 6 h and longer, the ferroelectric switching was largely suppressed. Obviously, ferroelectric switching was enhanced at high temperatures, primarily owing to the weaker hydrogen-bonding strength in glassy Selar.

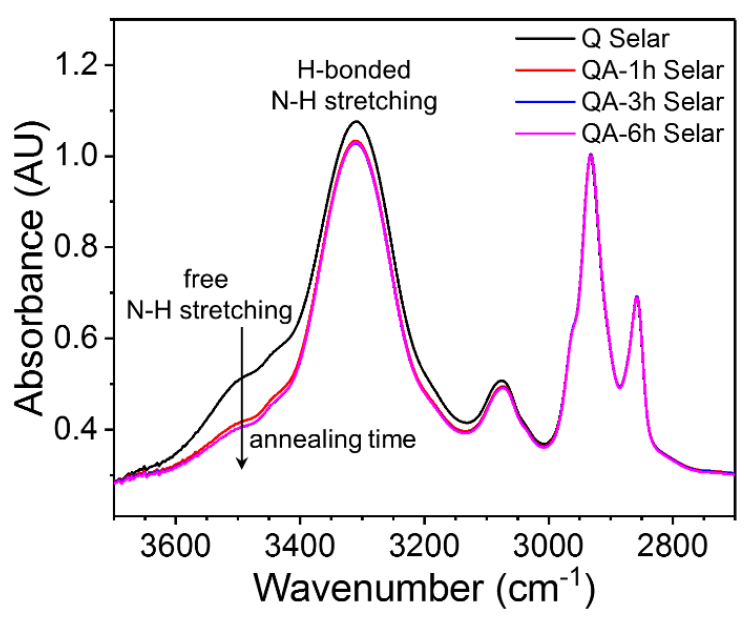


Figure 5. FTIR spectra for Q and QA Selar films at room temperature. The FTIR experiment was performed on the same Q film, which was annealed in-situ at 110 °C for different lengths of time.

The hydrogen-bonding strength was studied by FTIR. Figure 5 shows FTIR spectra in the range of 3700-2700 cm⁻¹ for the Q and QA Selar films. The same Q film was subjected to an insitu annealing at 110 °C for different lengths of time. For each data collection, the sample was cooled to RT to ensure a valid comparison of different spectra, i.e., the absorption bands for asymmetric/symmetric CH₂ stretching bands overlapped nicely. The Q Selar film exhibited a relatively broad hydrogen-bonded N-H stretching band centered at 3310 cm⁻¹, together with some shoulder bands around 3500 cm⁻¹ for the free N-H stretching band.^{46,47} This result suggested that hydrogen-bonding in Q Selar was relatively weak with certain non-bonded amide groups. After annealing at 110 °C for 1 h, the shoulder bands for free N-H stretching around 3500 cm⁻¹ clearly reduced their intensity. With further increasing the annealing time, the intensity decreases became less obvious for the QA-3h and QA-6h films. Meanwhile, there was also a decrease in the hydrogen-bonded N-H stretching band at 3310 cm⁻¹ for the QA films compared to the Q film. The attenuation in this N-H stretching band indicated that more amide groups were better hydrogen-

bonded in the QA Selar films due to thermal annealing.^{46, 47} From this FTIR study, it is clear that non-bonded amide groups and weak hydrogen-bonding interaction facilitated ferroelectric switching in the Q Selar film. After thermal annealing, ferroelectric response was substantially suppressed due to strengthened hydrogen-bonds in QA films; the longer the annealing time, the stronger the hydrogen-bonding interaction in the glassy nylon. Meanwhile, free volume in the polymer glass also decreased. As a result, either a higher electric field or a higher temperature was required to break the hydrogen bonds and induce ferroelectric switching for QA Selar films.

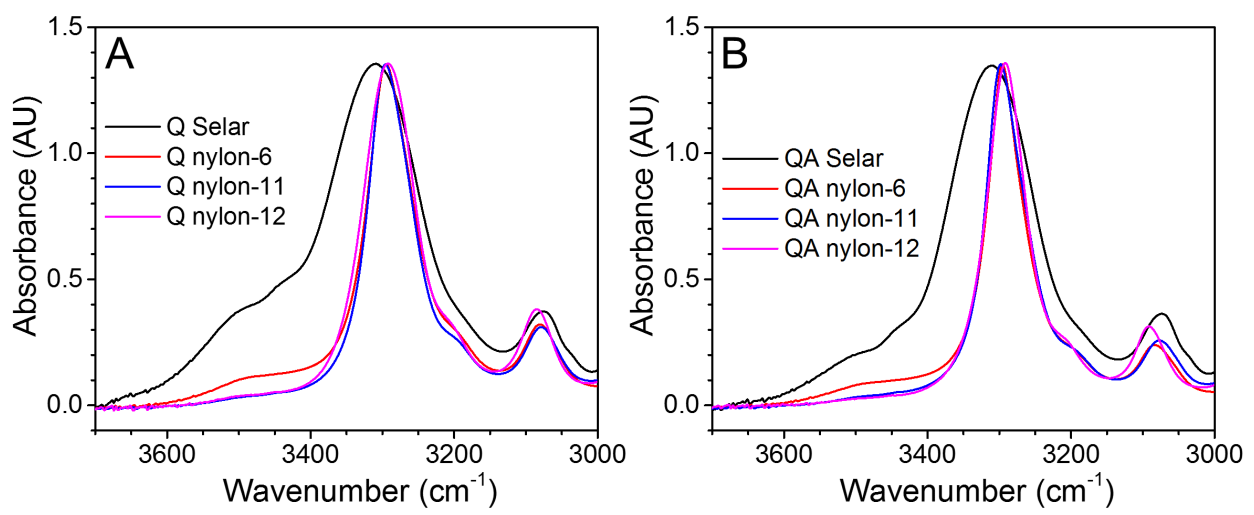


Figure 6. FTIR spectra for various (A) Q and (B) QA nylon films at room temperature. All spectra are normalized to the hydrogen-bonded N-H stretching band around 3310 cm⁻¹. The QA Selar is QA-6h.

Comparison with the Amorphous Phase in Aliphatic Nylons. As discussed earlier, the glassy phase in aliphatic nylons does not contribute much to the observed ferroelectric behavior. Then, what is the difference between the glassy phases in aliphatic and aromatic nylons? Why do they behave so differently in ferroelectric switching? To answer these questions, a comparison study was carried out for various aliphatic *n*-nylons. First, all Q *n*-nylons exhibited a broad amorphous halo-like scattering around 14.7 nm⁻¹ (0.427 nm) in WAXD,³² whereas Q Selar showed

an amorphous halo at 14.5 nm⁻¹ (0.433 nm, see Figure 1). The slightly larger average interchain distance for Q Selar suggested that the chain packing in the glassy Selar was looser than that in the glassy phase of *n*-nylons. This could be attributed to the aromatic rings in Selar. Second, Figure 6A compares the normalized FTIR spectra for Q Selar and Q n-nylons at room temperature, and obvious differences are observed. All Q n-nylons exhibited narrower hydrogen-bonded N-H stretching bands than Q Selar, and their positions appeared at a lower wavenumber (3295 cm⁻¹) than that (3310 cm⁻¹) for Q Selar. Moreover, the absorption of the free N-H stretching band around 3500 cm⁻¹ was much stronger for Q Selar than that for Q *n*-nylons. From these results, we conclude that there were more non-bonded amide groups and the hydrogen-bonding strength was weaker in Q Selar than Q n-nylons. After thermal annealing, the N-H stretching bands became narrower for all QA nylons (Figure 6B), suggesting strengthened hydrogen-bonding and a reduced amount of non-bonded amide groups. However, differences between QA Selar and QA n-nylons were still obvious. The broader hydrogen-bonded N-H stretching band for QA Selar than those for QA nnylons suggested much weaker hydrogen-bonding interaction in QA Selar. experimental results, we conclude that weaker hydrogen-bonding and looser chain packing in glassy aromatic Selar resulted in easier ferroelectric switching than the glassy phases in aliphatic nylons.

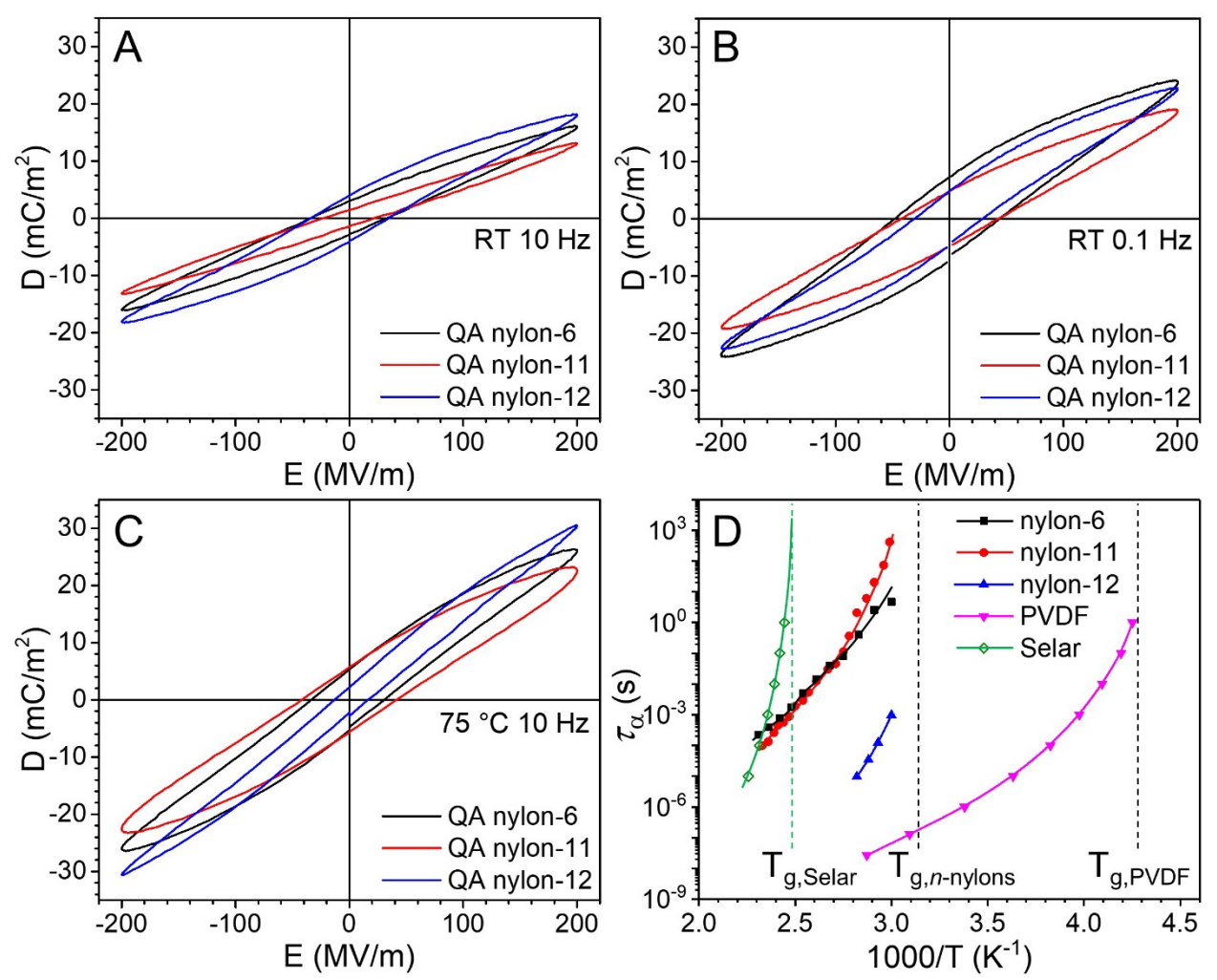


Figure 7. (A-C) Bipolar D-E loops for various QA *n*-nylons at (A) RT/10 Hz, (B) RT/0.1 Hz, and (C) 75 °C/10 Hz, respectively. The poling field was 200 MV/m with a sinusoidal waveform. (D) The α relaxation time (τ_{α}) as a function of 1/T for various *n*-nylons and PVDF. The relaxation data for dry nylon-6, nylon-11, nylon-12, and PVDF samples are taken from refs. 48, 49, 50, and 53, respectively.

Given the strong hydrogen-bonding and tight chain packing in n-nylons, their glassy phases supposedly should not show ferroelectric switching below T_g . However, this is not true, and QA n-nylons were chosen to study the ferroelectric switching of their amorphous phases. Prior WAXD results revealed that the QA n-nylon films contained the most stable crystalline forms; α form for the QA nylon-6 film, α form for the QA nylon-11 film, and γ form for the QA nylon-12 film (see the Supporting Information in ref. 32). Because these stable crystalline forms had strong

hydrogen-bonding with tight crystal packing, possible interference of ferroelectric switching from the mesophases could be largely avoided. Figure 7A shows the bipolar D-E loops for QA *n*-nylons under 10 Hz at RT (i.e., below T_g; note that the T_g values for nylon-6, nylon-11, and nylon-12 are between 45 and 55 °C ³²). The QA nylon-11 showed a linear loop with the lowest D_{max}, the QA nylon-12 showed the broadest (i.e., ferroelectric-like) D-E loop with the highest D_{max}, and the QA nylon-6 displayed a D-E loop between the two cases. Obviously, the glassy phases in QA nylon-12 and nylon-6 exhibited limited ferroelectric switching with certain dipole saturation at the maximum poling field. When the poling frequency decreased to 0.1 Hz (Figure 7B), more pronounced ferroelectric switching was seen for all n-nylons with QA nylon-6 exhibiting the broadest loop. However, compared to quenched n-nylons, the ferroelectric switching was much weaker ($D_{\text{max}} \sim 20 \text{ mC/m}^2$) than that ($D_{\text{max}} > 50 \text{ mC/m}^2$) from mesomorphic *n*-nylons. We consider that the glassy phases can exhibit weak ferroelectric switching, especially when the poling frequency is low and/or the poling field is high. When the temperature increased to 75 °C (above T_g, Figure 7C; the AC electronic conduction was subtracted for all loops, see Figure S4), a slim loop with the highest D_{max} was observed for the QA nylon-12, which appeared more paraelectric than ferroelectric. By contrast, the QA nylon-11 exhibited the broadest loop with the lowest D_{max} , which looked more ferroelectric than paraelectric. Again, the loop for the QA nylon-6 was between the two cases.

From Figures 7A/C, differences are seen for the amorphous phases in nylon-6, nylon-11, and nylon-12; the D_{max} decreases in the order of nylon-12 > nylon-6 > nytlon-11. This trend suggests that the polarizability of the amorphous phase should also decrease in the sequence of nylon-12 > nylon-6 > nylon-11. Different ferroelectric behaviors of the amorphous phases in n-nylons can be correlated to their α relaxation times (τ_{α}); see Figure 7D. These τ_{α} values are

obtained for dry samples from literature reports: ref. 48 for nylon-6, ref. 49 for nylon-11, and ref. 50 for nylon-12. Close to the T_g of *n*-nylons, the τ_{α} decreases in the order of nylon-11 > nylon-6 > nylon-12, and the difference between the τ_{α} values for nylon-11 and nylon-12 is over 5 orders of magnitude. Given only one methylene unit difference in their chemical structures, it is surprising to see such different τ_{α} values for nylon-11 and nylon-12. The odd-even effect for aliphatic nnylons can be used to explain. When arranged in an all trans conformation, the amide dipoles are parallel for odd-numbered n-nylons, whereas they are antiparallel for even-numbered n-nylons. More importantly, in α nylon-11 ⁵¹ and γ nylon-12 crystals, ⁵² adjacent amide dipoles in neighboring chains are parallel for nylon-11 and antiparallel for nylon-12 in the unit cells. We speculated that similar situations could also happen for amorphous *n*-nylons. Namely, amorphous odd-numbered nylons may prefer a parallel arrangement for neighboring interchain amide dipoles, while amorphous even-numbered nylons prefer an antiparallel arrangement. According to the Fröhlich-Kirkwood theory,²⁰ when neighboring inter-chain dipoles arrange in a parallel scheme, the g factor will be high and the dipole-dipole interaction will be strong. On the contrary, when neighboring inter-chain dipoles arrange in an antiparallel scheme, the g factor will be low and the dipole-dipole interaction will be weak. If this speculation is true, the intermolecular (hydrogenbonding) interaction is stronger in odd-numbered nylon-11 than even-numbered nylon-12 (and possibly nylon-6). It should be the stronger hydrogen-bonding in nylon-11 that results in a much longer τ_{α} or lower segmental polarizability for amorphous nylon-11 than amorphous nylon-12. The longer τ_{α} and the lower segmental polarizability for nylon-6 than nylon-12 can be attributed to the higher dipole density and thus stronger hydrogen-bonding in amorphous nylon-6. We consider that the weaker hydrogen-bonding interaction in nylon-12 should persist below Tg; as such, glassy nylon-12 is easier to exhibit ferroelectric switching than glassy nylon-6 and nylon-11.

When the temperature is around and slightly above T_g , the stronger hydrogen-bonding interaction and thus lower dipole polarizability in nylon-6 and nylon-11 can enable certain ferroelectric switching induced by the high poling electric field, especially at low frequencies. In Figure 7D, the τ_{α} values for poly(vinylidene fluoride) (PVDF) are much shorter than those for *n*-nylons at the same temperature.⁵³ This is attributed to its lower T_g (-37 °C) and weaker dipolar interaction than the hydrogen-bonding in *n*-nylons. Therefore, around RT, the amorphous PVDF phase does not show any ferroelectric switching at all. The above speculation and discussion certainly will need more direct proof from future studies such as computer simulation.

The Nature of Ferroelectric Switching in Glassy Nylons. First of all, ferroelectric switching in glassy polymers is different from that in the crystalline phase, because chains are more or less randomly packed in the amorphous phase whereas they are at least aligned in the crystalline phase. In the crystalline phase, ferroelectric switching is realized via cooperative (i.e., domain) rotation of the polar chains (note that dipoles are orthogonal to the polymer chain, such as in PVDF and nylons). 54,55 Obviously, this cooperative rotation of aligned chains is not possible for glassy polymers. Second, it is unlikely that the α transition temperature can be significantly decreased by high poling electric field. Instead, ferroelectric switching should be facilitated by sub-T_g relaxations.¹² In general, for main-chain polar polymers [i.e., polar groups are directly attached to the main chain, e.g., PVDF, polycarbonate (PC), polysulfone (PSF), polyesters, and nylons], the β relaxation is usually related to the onset or precursors of long-range segmental motions (i.e., the α relaxation), and thus can be considered as short-range segmental motions. The γ relaxation occurs at a lower temperature and is related to the motion of progressively localized moieties of the chain. For side-chain polar polymers (i.e., polar groups are attached to the side chains, such as polyacrylates and polymethacrylates), the β transition directly relates to the

localized motion of dipole groups in the side chains. For glassy nylons, it is not yet clear which sub-T_g relaxation is primarily responsible for the ferroelectric switching. Below, we will use HV-BDS to answer this question.

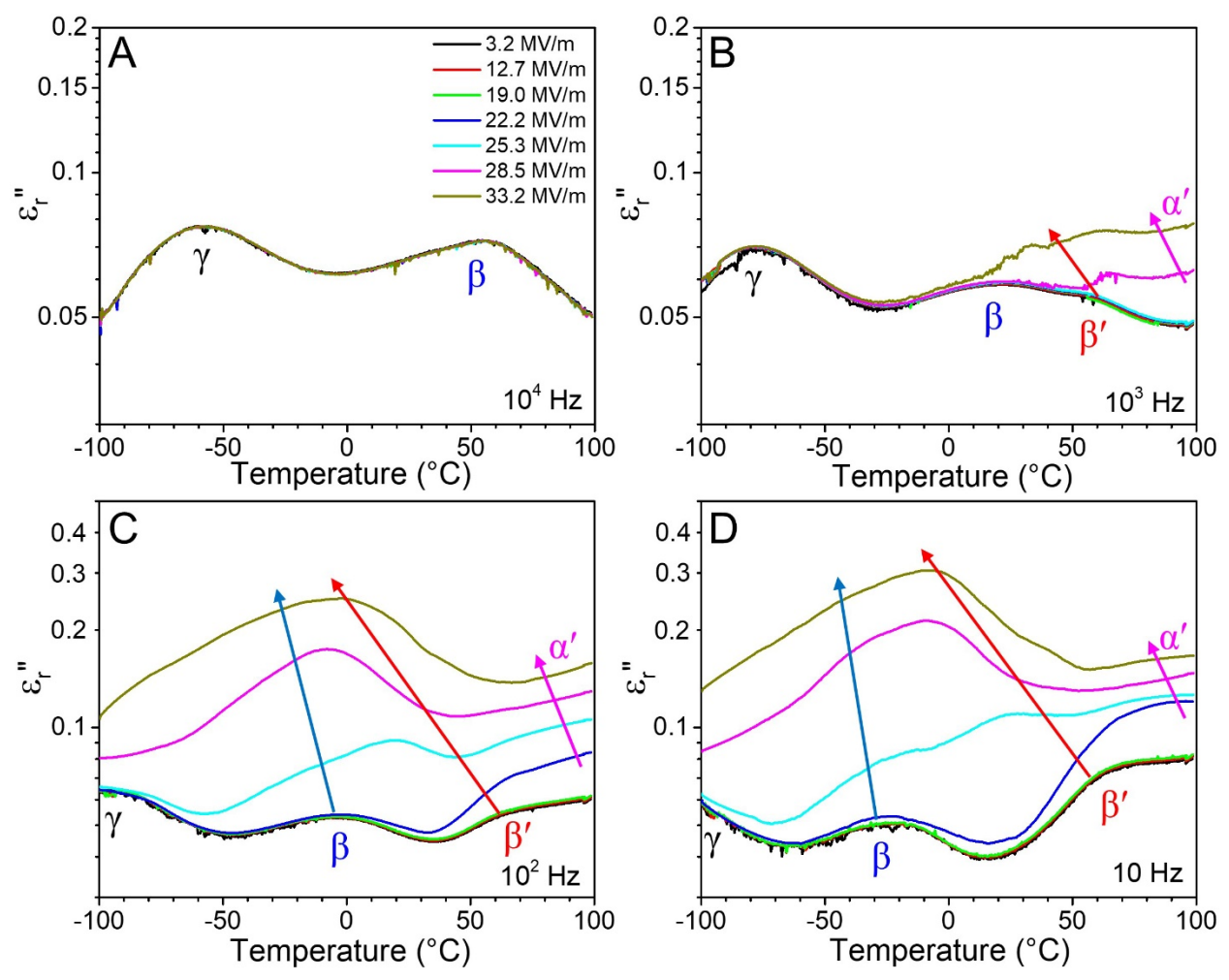


Figure 8. HV-BDS temperature-scan $ε_r$ " results for the Q Selar film under different electric fields at (A)10⁴ Hz, (B)10³ Hz, (C)10² Hz, and (D) 10 Hz. The heating rate was 0.3 °C/min. The arrows suggest the trend of sub-T_g transition changes as the applied electric field increases.

Different relaxation processes associated with motions of amide groups can be found in the normal BDS results in Figure S5. The γ relaxation was assigned to the local motion of methylene units adjacent to the amide groups. The β relaxation was assigned to the motion of the water-bonded amide groups (i.e., from absorbed moisture). This relaxation disappeared during the

second heating process, because water was evaporated after heating to 140 °C. The α relaxation was found around 130 °C. Between the β and α relaxations, there was another relaxation peak for the Q Selar film, which persisted even during the second heating of the dried sample. We named it as β' , which could be considered as the precursor motion for the α relaxation, although its exact origin was still unclear.

Figure 8 shows HV-BDS temperature-scan ε_r " results for Q Selar film under different frequencies and electric fields (the $\varepsilon_{\rm r}$ ' results are shown in Figure S6). At 10^4 Hz (Figure 8A), the γ and β relaxations were observed with no electric field dependence. With decreasing the frequency to 10^3 Hz (Figure 8B), the β' relaxation appeared around 60 °C, and it gradually shifted to lower temperatures with an increased amplitude upon increasing the electric field to above 28 MV/m. In addition, the ε_r around 70-100 °C also significantly increased. Since this temperature range was below the T_g around 130 °C, this increase in ε_r " could not be assigned to the glass (or α) transition. As reported before, even below T_g, there still exists certain long-range segmental motion, which is similar to the glass transition motion. ^{56, 57} It is this glass transition-like segmental motion below Tg that causes the flow and plastic deformation of polymer glasses. Here, we name it as the field-induced α' transition. We consider that it was likely that the high electric field enhanced this type of long-range segmental motion even below T_g. When frequency decreased to 10^2 (Figure 8C) and 10 Hz (Figure 8D), all relaxation modes started to increase in $\epsilon_{r}{''}$ with increasing the electric field; however, the enhancement of β and β' relaxations appeared to be the more significant than that of the α' relaxation. Considering that high poling electric field tends to make dipole switching easier, these relaxation should shift to lower temperatures as the poling field increased.

Similar HV-BDS study was also performed for the Q nylon-11 film (see Figures S7 and S8). From the ϵ_r " results in Figure S8, similar trends could be seen. First, when the frequency was 10^4 Hz (Figure S8A), no field dependence could be observed for the γ (the local motion of methylene units adjacent to the amide groups), β (the motion of water-bonded amide), and α (the glass transition) relaxations. When the frequency decreased to 10^3 Hz (Figure S8B), γ , β , and α' motions significantly enhanced when the field was above 25.3 MV/m, whereas there was not much change for the α motion. When the frequency decreased to below 10^2 Hz (Figures S8C,D), β and α' gradually shifted to lower temperatures upon increasing the electric field. Although the α relaxation enhanced, the position remained nearly constant, suggesting that the glass transition was not much altered by the poling field.

From the above HV-BDS result, we conclude that ferroelectric switching in glassy Selar is primarily enabled by the cooperative segmental motions from β/β' and α' relaxations (note that the γ contribution is minor in this case). In addition, the disappearance of field-induced ferroelectric domains (see Figure 4B) should also be realized via sub-T_g relaxations, rather than the α relaxation. This is because the τ_{α} for Selar around 75 °C can be extrapolated to beyond 10^5 s (see Figure 7D), much longer than the τ_{d} (~50 s) of P_r at 75 °C (Figure 4B). Also, the α' relaxation should not exist after removal of the electric field. Therefore, the decay of P_r after removal of poling field should be primarily attributed to the short-range segmental motions, i.e., β/β' , in glassy Selar.

Comparison of Ferroelectric Behaviors in Glassy Aromatic Nylons and Mesomorphic Even-Numbered Nylons. From the above studies, the ferroelectric behavior of glassy aromatic nylons has certain similarities with that of mesomorphic even-numbered aliphatic nylons. Before electric poling, no ferroelectric domain exists in the sample. The weak hydrogen-bonding and enlarged interchain distance enables large-angle rotation of the amide dipoles when a high poling

field is applied. As more amide dipoles participate in the cooperative rotation, transient (or dynamic) ferroelectric domains form. The domain size depends on the hydrogen-bonding strength and dipole polarizability. The stronger the hydrogen-bonding and the higher dipole polarizability, the larger the ferroelectric domains and thus the broader the hysteresis loop. Usually, hydrogen-bonding is sensitive to temperature. The higher the temperature, the slimmer the hysteresis loop.

These field-induced ferroelectric domains are metastable in nature, because there is no polar crystalline structure to stabilize them. Therefore, they have a relatively short lifetime as soon as the external electric field is removed. The lifetime depends on the dipole relaxation processes, which are sensitive to temperature; the higher the temperature, the faster the dipole relaxation or depolarization occurs. In this sense, glassy aromatic nylons and mesomorphic even-numbered nylons are not suitable for ferroelectric memory applications.⁵⁸

There is a clear difference between glassy aromatic nylons and mesomorphic evennumbered nylons. For a glassy aromatic nylon (i.e., a main-chain dipolar glass polymer), the segmental dipole rotation (i.e., the β/β' and α' motions) contributes significantly to the ferroelectric switching, and the contribution from localized γ motion is minor. This is why no significant ferroelectric switching reported for side-chain dipolar glass polymers, ^{11, 18} which do not possess any short-range segmental motion. For mesomorphic even-numbered nylons, cooperative rotation of aligned chains in the crystalline structure contribute to the ferroelectric switching. To certain extent, ferroelectric switching in mesomorphic even-numbered nylons could be easier than that in glassy aromatic nylons because polymer chains are aligned in the crystalline phase.

Conclusions and Outlook

In this work, the nature of ferroelectric switching in glassy aromatic nylons was investigated using a nearly 100% amorphous nylon, Selar. Similar to mesomorphic evennumbered n-nylons, hydrogen-bonding interaction and interchain distance played an important role for the ferroelectric switching in Selar. WAXD results revealed that the Q Selar had a larger average interchain distance than that in Q n-nylons because of aromatic rings in the main chain. FTIR results showed that the Q Selar exhibited a higher fraction of free amide groups than the QA Selar, and the hydrogen-bonding interaction in Q and QA Selar was much weaker than that in aliphatic *n*-nylons. The weak hydrogen-bonding in Q Selar facilitated ferroelectric switching, which was largely suppressed for the QA Selar films. The ferroelectric domains were induced by the poling field, and thus were metastable and short-lived. The nature of ferroelectric switching was revealed by HV-BDS. Upon increasing the applied electric field, the segmental motions, i.e., β/β' and α' relaxations, contributed significantly to the dielectric loss, suggesting that the ferroelectric switching was primarily caused by the cooperative segmental motions in Selar. In addition, absorption of moisture was detrimental to the dielectric properties of dipolar glass nylons, because the β relaxation became easier and often took place at lower temperatures. Absorbed moisture tended to significantly decrease the dielectric breakdown strength.

Once we understand the nature of ferroelectric switching in aromatic nylons, it is desirable to suppress segmental motions for high energy density and low loss dielectric applications. Several strategies are proposed for future studies. First, extended thermal annealing can be used to strengthen hydrogen-bonding and decrease the free volume for glassy nylons. Second, crystallinity can be introduced into the aromatic nylons to enhance hydrogen-bonding. Combining with extended thermal annealing, semicrystalline aromatic nylons could suppress ferroelectric

switching. In this sense, semicrystalline MXDs could be a viable candidate. Third, instead of

semi-aromatic nylons (i.e., either diamine or diacid is aromatic), fully aromatic nylons (i.e., both

diamine and diacid are aromatic) can be promising, e.g., copolymers from m-xylylenediamine and

I/T (a fully aromatic nylon commercialized by Mitsubishi).⁵⁹ Currently, research is on the way to

test these ideas.

Author Information

Corresponding Author

*E-mail: lxz121@case.edu (L.Z.).

Acknowledgement

This work is supported by National Science Foundation (DMR-1402733).

acknowledges financial support from China Scholarship Council.

Supporting Information. The Supporting Information is available free of charge on the

ACS Publications website at DOI: xxxxxxxxxxxxxxx

Continuous bipolar D-E loops for the QA Selar films at RT and 75 °C, DSC curves for the

QA Selar films and continuous bipolar D-E loops for the CA Selar film, subtraction of AC

electronic conduction from bipolar D-E loops for the QA *n*-nylons at 75 °C, normal BDS results

for the Q Selar film, and HV-BDS temperature-scan results for Q Selar and QA nylon-11 films.

29

References

- 1. Zhu, L. Exploring strategies for high dielectric constant and low loss plolymer dielectrics. *J. Phys. Chem. Lett.* **2014**, *5*, 3677-3687.
- 2. Chen, Q.; Shen, Y.; Zhang, S.; Zhang, Q. M. Polymer-based dielectrics with high energy storage density. *Annu. Rev. Mater. Res.* **2015**, *45*, 433-458.
- 3. Baer, E.; Zhu, L. 50th Anniversary Perspective: Dielectric phenomena in polymers and multilayered dielectric films. *Macromolecules* **2017**, *50*, 2239-2256.
- 4. Carpi, F.; De Rossi, D.; Kornbluh, R.; Pelrine, R. E.; Sommer-Larsen, P. Dielectric Elastomers as Electromechanical Transducers: Fundamentals, Materials, Devices, Models And Applications of An Emerging Electroactive Polymer Technology; Elsevier: Boston, MA, 2008.
- 5. Brochu, P.; Pei, Q. Advances in dielectric elastomers for actuators and artificial muscles. *Macromol. Rapid Commun.* **2010**, *31*, 10-36.
- 6. Zhang, Q.; Huang, C.; Xia, F.; Su, J. Electric EAP. In *Electroactive Polymer (EAP) Actuators* as *Artificial Muscles: Reality, Potential, and Challenges*, 2nd ed.; Bar-Cohen, Y., Ed.;. SPIE Press: 2004, Chapter 4.
- 7. Neese, B.; Chu, B.; Lu, S. G.; Wang, Y.; Furman, E.; Zhang, Q. Large electrocaloric effect in ferroelectric polymers near room temperature. *Science* **2008**, *321*, 821-823.
- 8. Moya, X.; Kar-Narayan, S.; Mathur, N. D. Caloric materials near ferroic phase transitions.

 Nat. Mater. 2014, 13, 439-450.
- 9. Correia, T.; Zhang, Q. *Electrocaloric Materials: New Generation of Coolers*; Springer: New York, 2013.

- Zhu, L.; Wang, Q. Novel ferroelectric polymers for high energy density and low loss dielectrics. *Macromolecules* 2012, 45, 2937-2954.
- 11. Wei, J.; Zhang, Z.; Tseng, J.-K.; Treufeld, I.; Liu, X.; Litt, M. H.; Zhu, L. Achieving high dielectric constant and low loss property in a dipolar glass polymer containing strongly dipolar and small-sized sulfone groups. *ACS Appl. Mater. Interfaces* **2015**, *7*, 5248-5257.
- Fried, J. R. Sub-T_g transitions. In *Physical Properties of Polymers Handbook*; Mark, J. E.,
 Ed.; Springer: New York, 2007; Vol. 13, pp 217-232.
- Bendler, J. T.; Boyles, D. A.; Edmondson, C. A.; Filipova, T.; Fontanella, J. J.; Westgate, M. A.; Wintersgill, M. C. Dielectric properties of bisphenol a polycarbonate and its tethered nitrile analogue. *Macromolecules* 2013, 46, 4024-4033.
- 14. Tasaka, S.; Inagaki, N.; Miyata, S.; Chiba, T. Electrical properties of cyanoethylated polysaccharides. *Sen'i Gakkaishi* **1988**, *44*, 546-550.
- 15. Sato, T.; Tsujii, Y.; Kita, Y.; Fukuda, T.; Miyamoto, T. Dielectric-relaxation of liquid-crystalline cyanoethylated *o*-(2,3-dihydroxypropyl)cellulose. *Macromolecules* **1991**, *24*, 4691-4697.
- 16. Vandeleur, R. H. M. An extended analysis of the dielectric properties of poly[(2-cyanoethyl vinyl ether)-*co*-(vinyl alcohol)]. *Polymer* **1994**, *35*, 2691-2700.
- 17. Bedekar, B. A.; Tsujii, Y.; Ide, N.; Kita, Y.; Fukuda, T.; Miyamoto, T. Dielectric relaxation of cyanoethylated poly(2,3-dihydroxypropyl methacrylate). *Polymer* **1995**, *36*, 4735-4740.
- 18. Zhang, Z.; Wang, D. H.; Litt, M. H.; Tan, L.-S.; Zhu, L. High temperature and high energy density dipolar glass polymers based on sulfonylated poly(2,6-dimethyl-1,4-phenylene oxide). *Angew. Chem. Int. Ed.* **2018**, *57*, 1528-1531.

- 19. Treufeld, I.; Wang, D. H.; Kurish, B. A.; Tan, L.-S.; Zhu, L. Enhancing electrical energy storage using polar polyimides with nitrile groups directly attached to the main chain. *J. Mater. Chem. A* **2014**, *2*, 20683-20696.
- 20. Kao, K.-C. Dielectric Phenomena in Solids: with Emphasis on Physical Concepts of Electronic Processes; Elsevier Academic Press: Boston, MA, 2004.
- 21. Wu, S.; Li, W.; Lin, M.; Burlingame, Q.; Chen, Q.; Payzant, A.; Xiao, K.; Zhang, Q. Aromatic polythiourea dielectrics with ultrahigh breakdown field strength, low dielectric loss, and high electric energy density. *Adv. Mater.* **2013**, *25*, 1734-1738.
- 22. Wu, S.; Burlingame, Q.; Cheng, Z.; Lin, M.; Zhang, Q. Strongly dipolar polythiourea and polyurea dielectrics with high electrical breakdown, low loss, and high electrical energy density. *J. Electron. Mater.* **2014**, *43*, 4548-4551.
- Thakur, Y.; Dong, R.; Lin, M.; Wu, S.; Cheng, Z.; Hou, Y.; Bernholc, J.; Zhang, Q.
 Optimizing nanostructure to achieve high dielectric response with low loss in strongly dipolar polymers. *Nano Energy* 2015, 16, 227-234.
- 24. Thakur, Y.; Lin, M.; Wu, S.; Cheng, Z.; Jeong, D.; Zhang, Q. Tailoring the dipole properties in dielectric polymers to realize high energy density with high breakdown strength and low dielectric loss. *J. Appl. Phys.* 2015, 117, 114104.
- 25. Thakur, Y.; Zhang, B.; Dong, R.; Lu, W. C.; Iacob, C.; Runt, J.; Bernholc, J.; Zhang, Q. Generating high dielectric constant blends from lower dielectric constant dipolar polymers using nanostructure engineering. *Nano Energy* **2017**, *32*, 73-79.
- 26. Massey, L. K., Permeability Properties of Plastics and Elastomers: A Guide to Packaging and Barrier Materials. 2nd Ed.; William Andrew Pub.: Norwich, NY, 2003.

- 27. Koizumi, N. Ferroelectric behavior in polyamides constituted of ring systems. *Ferroelectrics* **1994**, *171*, 57-67.
- 28. Murata, Y.; Tsunashima, K.; Koizumi, N.; Ogami, K.; Hosokawa, F.; Yokoyama, K. Ferroelectric properties in polyamides of *m*-xylylenediamine and dicarboxylic acids. *Jpn. J. Appl. Phys.* **1993**, *32*, L849-L851.
- 29. Murata, Y.; Tsunashima, K.; Umemura, J.; Koizumi, N. Ferroelectric properties in aromatic polyamides. *IEEE 1994 Ann. Rep. Conf. Elect. Insul. Dielect. Phen.* **1994**, 779-784.
- Nagasawa, T.; Murata, Y.; Tsunashima, K.; Morishima, Y.; Yano, S.; Koizumi, N.
 Amorphous ferroelectric polyamide blends. *Macromolecules* 2000, 33, 2302-2304.
- 31. Nalwa, H. S. Ferroelectric nylons. In *Ferroelectric Polymers: Chemistry, Physics, and Applications*, Nalwa, H. S., Ed.; Marcel Dekker: New York, 1995; pp 281-323.
- 32. Zhang, Z.; Litt, M. H.; Zhu, L. Unified understanding of ferroelectricity in *n*-nylons: Is the polar crystalline structure a prerequisite? *Macromolecules* **2016**, *49*, 3070-3082.
- 33. Itoh, T.; Tanaka, T.; Hashimoto, M.; Konishi, T. Ferroelectric hysteresis behavior and structural property of even-numbered nylon film. *Jpn. J. Appl. Phys.* **1995**, *34*, 6164-6165.
- 34. Itoh, T.; Takano, M.; Yanagisawa, T.; Hashimoto, M. Ferroelectricity in odd- and evennumbered nylons. *Ferroelectrics* **1998**, *216*, 35-51.
- 35. Yanagisawa, T.; Itoh, T.; Hashimoto, M. Ferroelectricity and amorphous structure in quenched nylon 6 film. *Jpn. J. Appl. Phys.* **2001**, *40*, L1238-L1240.
- 36. Yanagisawa, T.; Itoh, T.; Saruyama, Y.; Fujiwara, S. Thermal, structural and ferroelectric properties of amorphous phases in quenched nylon 6 film. *J. Phys. Soc. Jpn.* **2004**, *73*, 2763-2767.

- 37. Kolesov, I.; Mileva, D.; Androsch, R.; Schick, C. Structure formation of polyamide 6 from the glassy state by fast scanning chip calorimetry. *Polymer* **2011**, *52*, 5156-5165.
- 38. Mollova, A.; Androsch, R.; Mileva, D.; Schick, C.; Benhamida, A. Effect of supercooling on crystallization of polyamide 11. *Macromolecules* **2013**, *46*, 828-835.
- 39. Scheinbeim, J. I.; Lee, J. W.; Newman, B. A. Ferroelectric polarization mechanisms in nylon 11. *Macromolecules* **1992**, *25*, 3729-3732.
- 40. Zhang, Z.; Litt, M. H.; Zhu, L. Understanding the paraelectric double hysteresis loop behavior in mesomorphic even-numbered nylons at high temperatures. *Macromolecules* **2017**, *50*, 5816-5829.
- 41. Aharoni, S. M. *n-Nylons: Their Synthesis, Structure, and Properties*; J. Wiley & Sons: New York, 1997.
- 42. Tashiro, K.; Kitai, H.; Saharin, S. M.; Shimazu, A.; Itou, T. Quantitative crystal structure analysis of poly(vinyl alcohol)-iodine complexes on the basis of 2D X-ray diffraction, raman spectra, and computer simulation techniques. *Macromolecules* **2015**, *48*, 2138-2148.
- 43. Murata, Y.; Tsunashima, K.; Koizumi, N. Dielectric hysteresis loop in alicyclic and aromatic polyamides. *Jpn. J. Appl. Phys.* **1994**, *33*, L354-L356.
- 44. Wunderlich, B. *Thermal Analysis of Polymeric Materials*; Springer: Berlin, 2005.
- 45. Jow, T. R.; Cygan, P. J. Dielectric breakdown of polyvinylidene fluoride and its comparisons with other polymers. *J. Appl. Phys.* **1993**, *73*, 5147-5151.
- 46. Skrovanek, D. J.; Howe, S. E.; Painter, P. C.; Coleman, M. M. Hydrogen bonding in polymers: Infrared temperature studies of an amorphous polyamide. *Macromolecules* **1985**, *18*, 1676-1683.

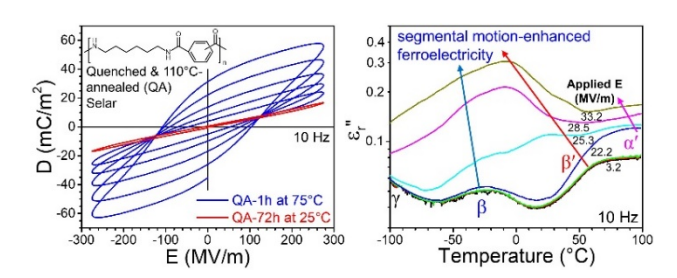
- 47. Skrovanek, D. J.; Painter, P. C.; Coleman, M. M. Hydrogen-bonding in polymers. 2. Infrared temperature studies of nylon-11. *Macromolecules* **1986**, *19*, 699-705.
- 48. Laredo, E.; Grimau, M.; Sanchez, F.; Bello, A. Water absorption effect on the dynamic properties of nylon-6 by dielectric spectroscopy. *Macromolecules* **2003**, *36*, 9840-9850.
- 49. Neagu, R. M.; Neagu, E.; Kyritsis, A.; Pissis, P. Dielectric studies of dipolar relaxation processes in nylon 11. *J. Phys. D: Appl. Phys.* **2000**, *33*, 1921-1931.
- 50. Pathmanathan, K.; Cavaille, J. Y.; Johari, G. P. The dielectric-properties of dry and water-saturated nylon-12. *J. Polym. Sci., Part B: Polym. Phys.* **1992**, *30*, 341-348.
- Newman, B. A.; Sham, T. P.; Pae, K. D. High-pressure X-ray study of nylon-11. *J. Appl. Phys.* 1977, 48, 4092-4098.
- Inoue, K.; Hoshino, S. Crystal-structure of nylon-12. *J. Polym. Sci., Part B: Polym. Phys.* 1973, 11, 1077-1089.
- 53. Yang, L.; Ho, J.; Allahyarov, E.; Mu, R.; Zhu, L. Semicrystalline structure dielectric property relationship and electrical conduction in a biaxially oriented poly(vinylidene fluoride) film under high electric fields and high temperatures. *ACS Appl. Mater. Interfaces* **2015**, *7*, 19894-19905.
- 54. Tashiro, K., Crystal structure and phase transition of PVDF and related copolymers. In *Ferroelectric Polymers: Chemistry, Physics, and Applications*; Nalwa, H. S., Ed.; Marcel Dekker: New York, 1995; pp 63-182.
- 55. Kepler, R. G., Ferroelectric, pyroelectric, and piezoelectric properties of poly(vinylidene fluoride). In *Ferroelectric Polymers: Chemistry, Physics, and Applications*; Nalwa, H. S., Ed.; Marcel Dekker, Inc.: New York, 1995; pp.183-232.

- 56. Yoshioka, S.; Aso, Y. Glass transition-related changes in molecular mobility below glass transition temperature of freeze-dried formulations, as measured by dielectric spectroscopy and solid state nuclear magnetic resonance. *J. Pharm. Sci.* **2005**, *94*, 275-287.
- 57. Hancock, B. C.; Shamblin, S. L.; Zografi, G. Molecular mobility of amorphous pharmaceutical solids below their glass-transition temperatures. *Pharm. Res.* **1995**, *12*, 799-806.
- 58. Naber, R. C. G.; Asadi, K.; Blom, P. W. M.; de Leeuw, D. M.; de Boer, B. Organic nonvolatile memory devices based on ferroelectricity. *Adv. Mater.* **2010**, *22*, 933-945.
- 59. Temin, S. C. Effect of structure on the glass temperature of polyamides. *J. Appl. Polym. Sci.* **1965**, *9*, 471-481.

TOC Graphic

Nature of Ferroelectric Behavior in Main-Chain Dipolar Glass Nylons: Cooperative Segmental Motion Induced by High Poling Electric Field

Zhongbo Zhang, Morton H. Litt, and Lei Zhu*



Supporting Information

Nature of Ferroelectric Behavior in Main-Chain Dipolar Glass Nylons: Cooperative Segmental Motion Induced by High Poling Electric Field

Zhongbo Zhang, Morton H. Litt, and Lei Zhu*

Department of Macromolecular Science and Engineering and Department of Chemistry, Case Western Reserve University, Cleveland, Ohio 44106-7202, United States

* Corresponding author. Email: lxz121@case.edu (L. Zhu)

I. Continuous Bipolar D-E Loops for the QA Selar Films at Room Temperature

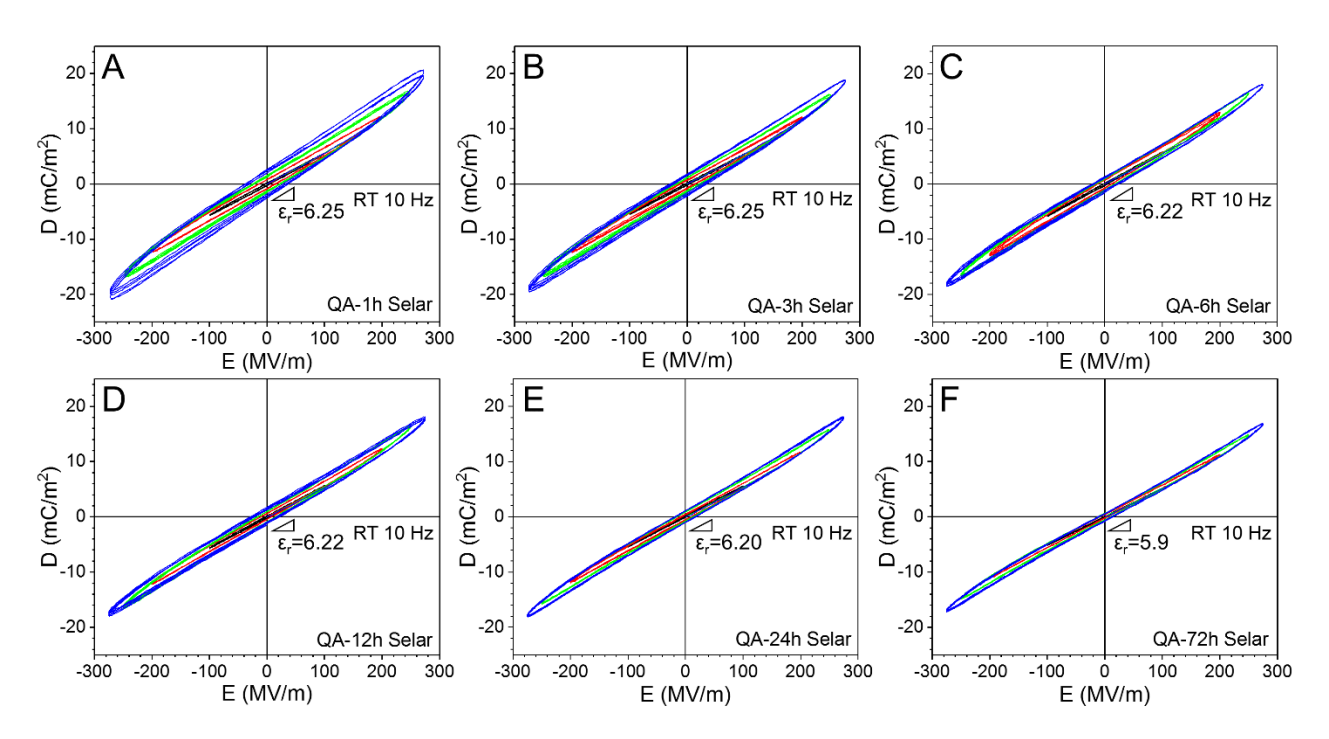


Figure S1. Continuous bipolar D-E loops (5 loops for each run) at room temperature for various QA Selar films under different electric fields; 100, 200, 250, and 275 MV/m. The poling frequency was 10 Hz with a sinusoidal waveform.

II. DSC Curves for QA Selar Films and Continuous Bipolar D-E Loops for the CA Selar Film

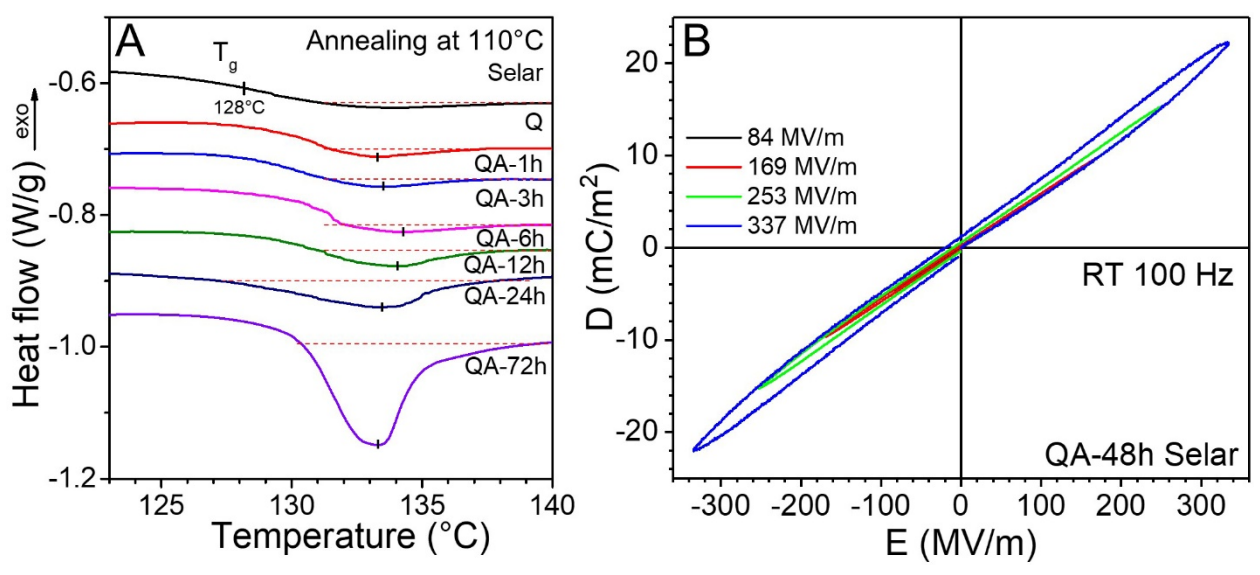


Figure S2. (A) First heating DSC thermograms for various QA Selar films. The heating rate was 10 °C/min. (B) Continuous bipolar D-E loops for the CA-72h Selar film with increasing the maximum poling field. The poling frequency was 100 Hz with a triangular waveform.

III. Continuous Bipolar D-E Loops for Various QA Selar Films at 75 °C

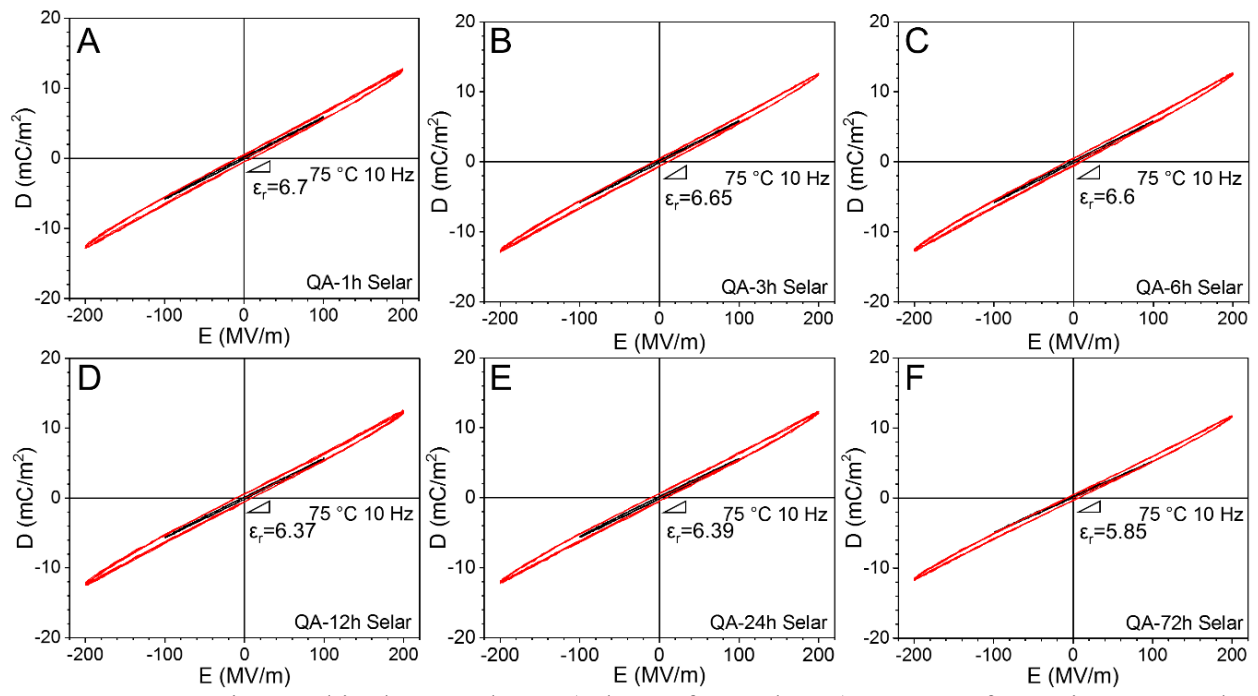


Figure S3. Continuous bipolar D-E loops (5 loops for each run) at 75 °C for various QA Selar films under different electric fields; 100 and 200 MV/m. The poling frequency was 10 Hz with a sinusoidal waveform.

IV. Subtraction of AC Electronic Conduction from Bipolar D-E Loops for the QA *n*-nylons at 75 °C

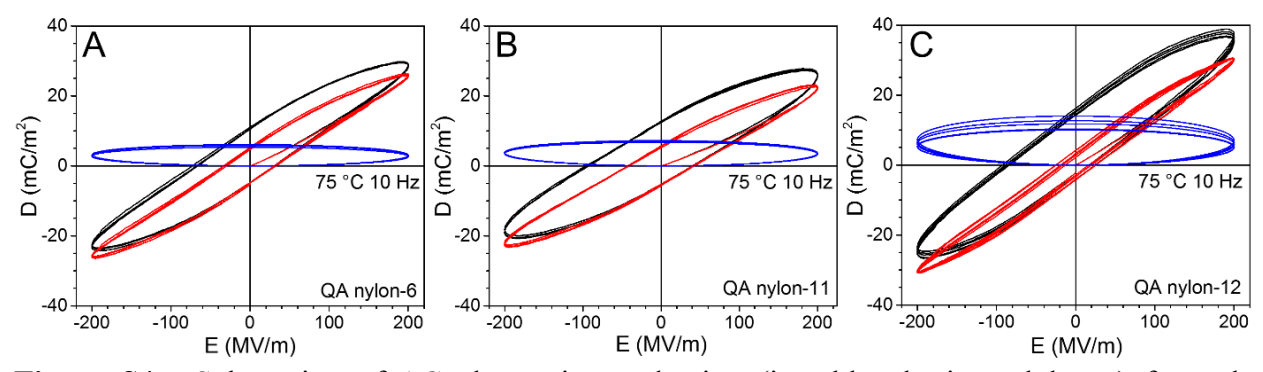


Figure S4. Subtraction of AC electronic conduction (i.e., blue horizontal loops) from the experimental (black) loops 75 °C for the QA (A) nylon-6, (B) nylon-11, and (C) nylon-12, respectively. The poling frequency was 10 Hz with a sinusoidal waveform.

At high temperatures, especially above the T_g of a polar polymer (usually with a high dielectric constant), charge (electron and/or hole) injection from metal electrodes becomes important when the poling electric field is above 20 MV/m, as evidenced by a thermally stimulated depolarization current (TSDC) study. During the bipolar poling, the electrode polarity alternates, and charge recombination happens if the traps near the metal/polymer interfaces are shallow. This leads to significant AC electronic conduction. In other words, the injected charges do not need to go through the entire film and the charge recombination near the metal/polymer interfaces can result in significant AC electronic conduction. As a result, the experimental D-E loops become asymmetric with respect to the origin along the D-axis. That is, the upper half loop shifts upward, as seen for the experimental (blank) loops in Figures S6. From our previous report, the AC electronic conduction results in a horizontal (blue) loop. After subtraction of the horizontal loop from the experimental loop, ferroelectric loops from dipole and domain switching can be obtained, as the red loops in Figure S6.

V. Normal BDS Temperature-Scan Results for the Q Selar Film

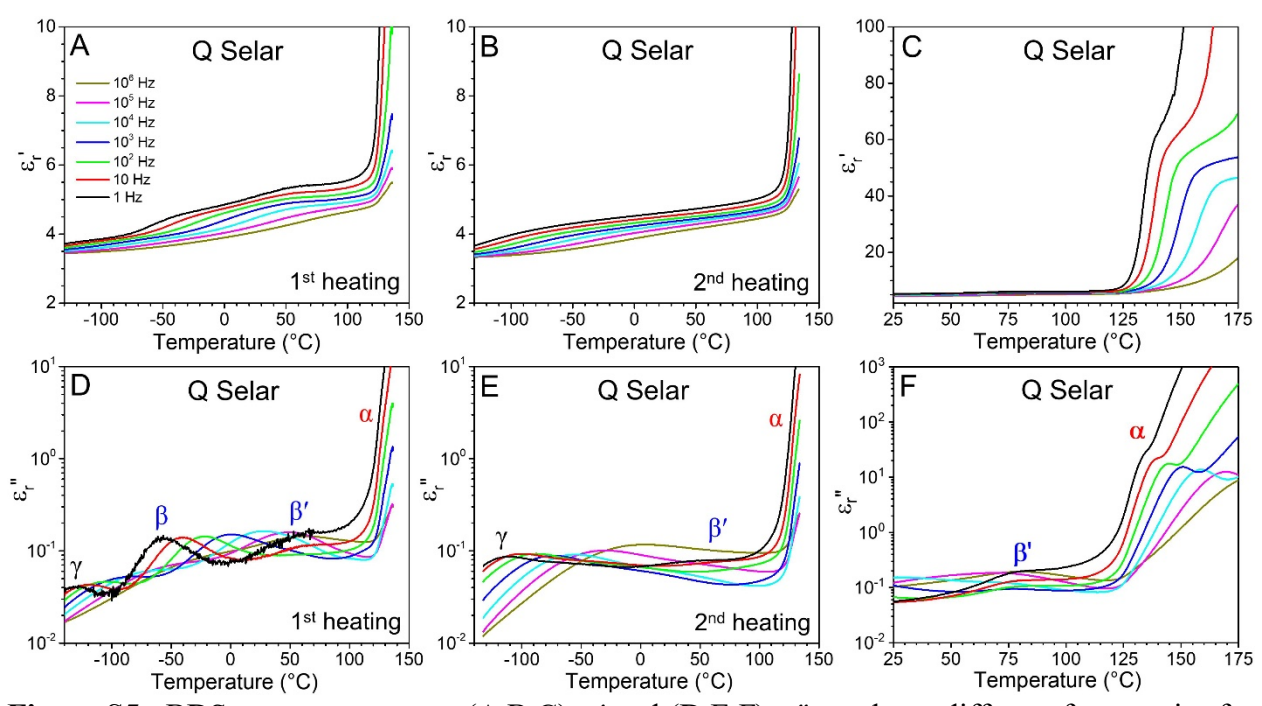


Figure S5. BDS temperature-scan (A,B,C) ϵ_{r}' and (D,E,F) ϵ_{r}'' results at different frequencies for the Q Selar film during (A/D and C/F) the first heating and (B,E) the second heating processes. The heating rate was 2 °C/min. Spectra in (C,F) show details for the α (or glass) transition.

VI. HV-BDS Temperature-Scan Results for Q Selar and QA Nylon-11 Films

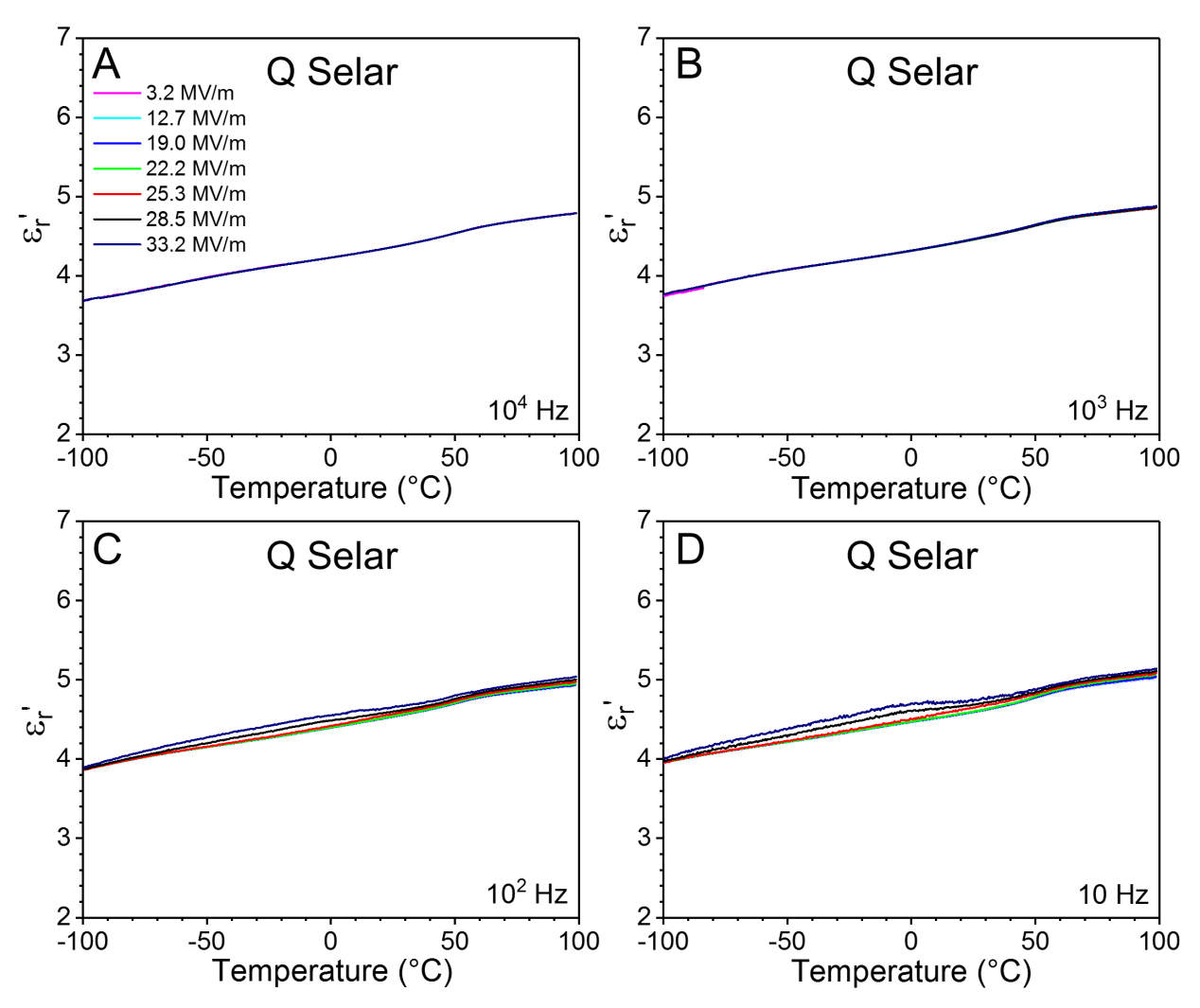


Figure S6. HV-BDS temperature-scan ε_r ' results for the Q Selar film under different electric fields at (A) 10^4 Hz, (B) 10^3 Hz, (C) 10^2 Hz, and (D) 10 Hz. The heating rate was 0.3 °C/min.

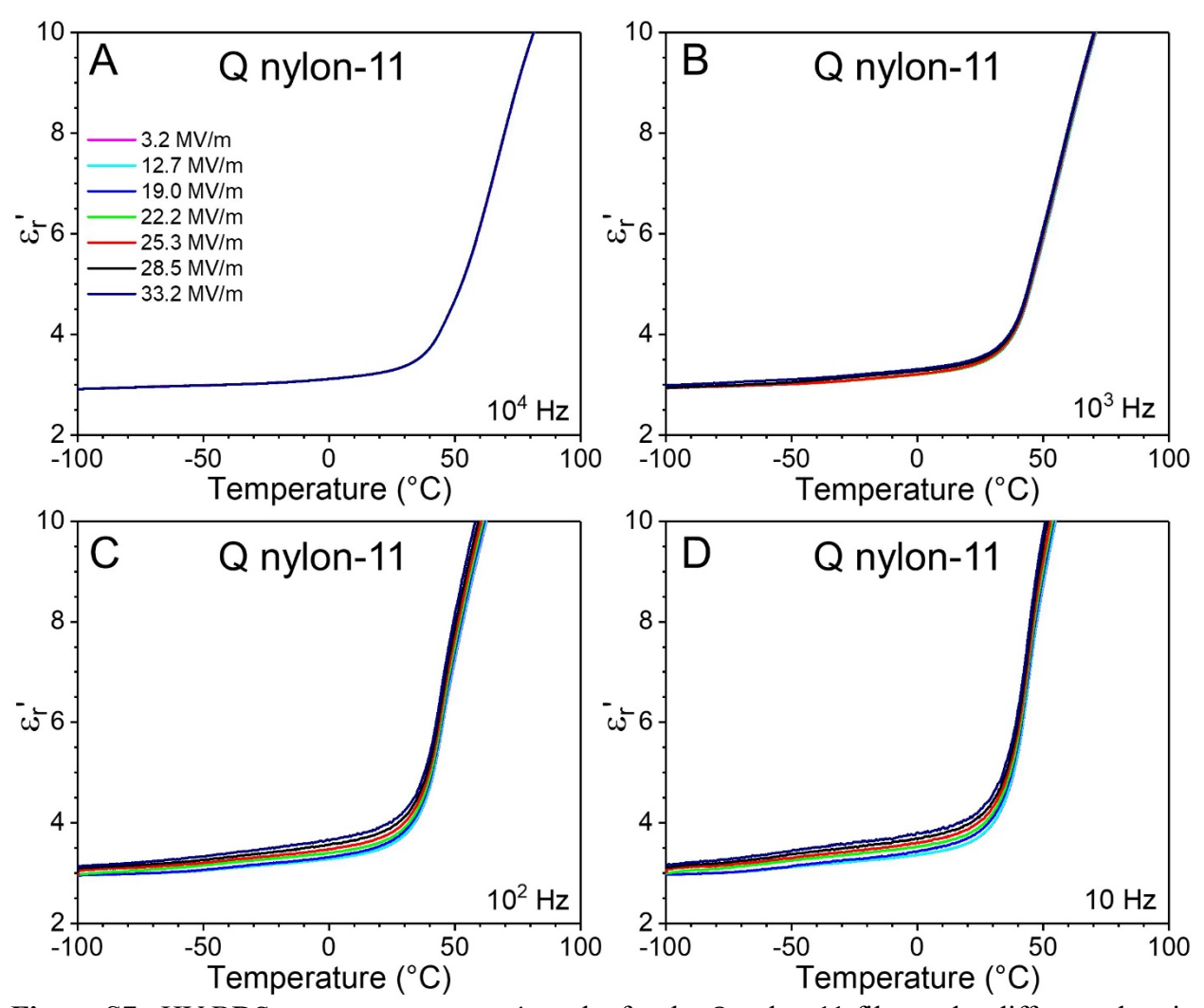


Figure S7. HV-BDS temperature-scan ϵ_r' results for the Q nylon-11 film under different electric fields at (A) 10^4 Hz, (B) 10^3 Hz, (C) 10^2 Hz, and (D) 10 Hz. The heating rate was 0.3 °C/min.

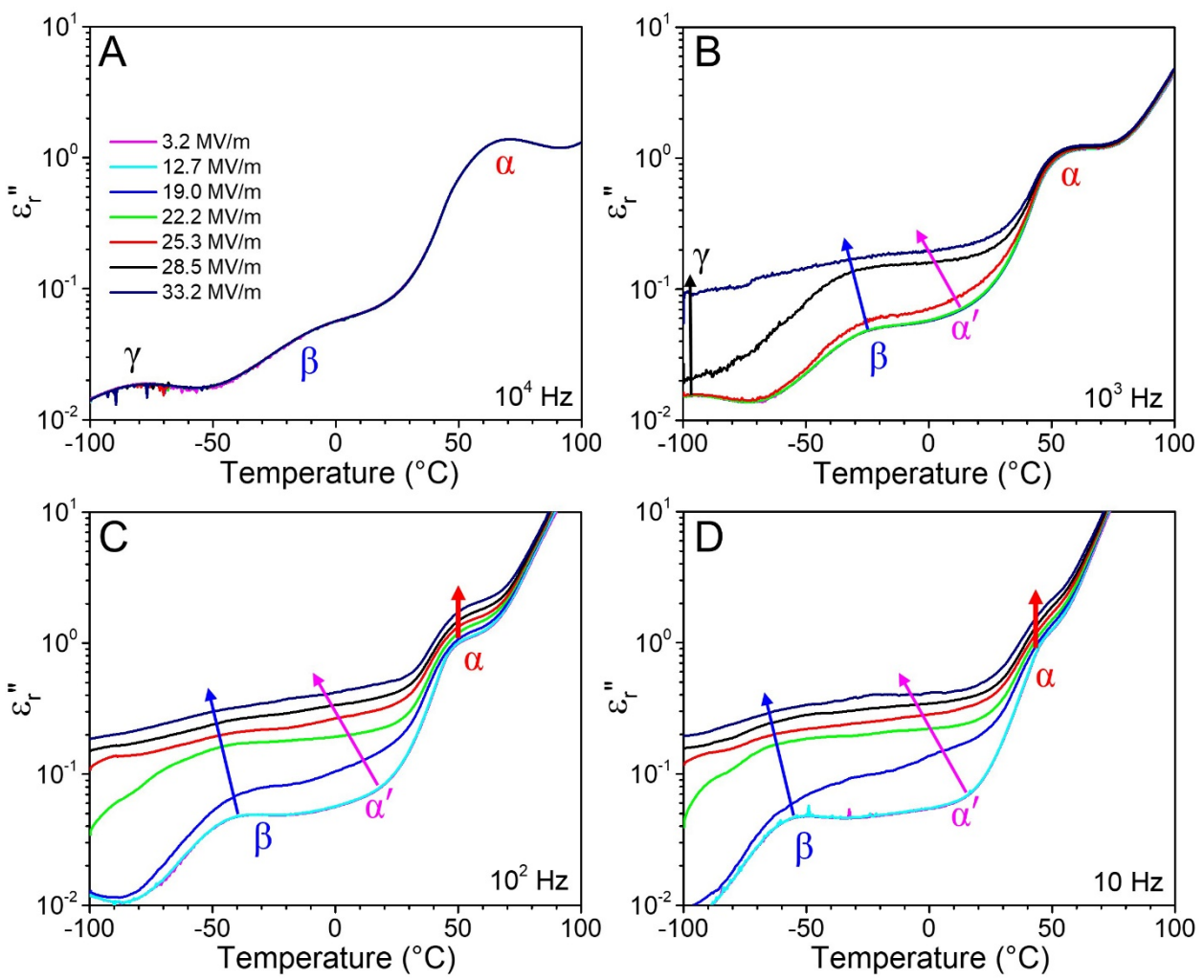


Figure S8. HV-BDS temperature-scan ϵ_r " results for the Q nylon-11 film under different electric fields at (A)10⁴ Hz, (B)10³ Hz, (C)10² Hz, and (D) 10 Hz. The heating rate was 0.3 °C/min. The arrows suggest the changes of sub-T_g transitions as the applied electric field increases.

References

- S1. Yang, L.; Ho, J.; Allahyarov, E.; Mu, R.; Zhu, L. Semicrystalline structure-dielectric property relationship and electrical conduction in a biaxially oriented poly(vinylidene fluoride) film under high electric fields and high temperatures. *ACS Appl. Mater. Interfaces* **2015**, *7*, 19894-19905.
- S2. Jow, T. R.; Cygan, P. J. Dielectric breakdown of polyvinylidene fluoride and its comparisons with other polymers. *J. Appl. Phys.* **1993**, *73*, 5147-5151.
- S3. Yang, L.; Allahyarov, E.; Guan, F.; Zhu, L., Crystal orientation and temperature effects on double hysteresis loop behavior in a poly(vinylidene fluoride-*co*-trifluoroethylene)-*graft*-polystyrene graft copolymer. *Macromolecules* **2013**, *46*, 9698-9711.